Reply on Anonymous Referee #1 (AMT-2017-50)

André Ehrlich[1], Eike Bierwirth[1,2], Larysa Istomina[3], and Manfred Wendisch[1]

[1]Leipzig Institute for Meteorology (LIM), University of Leipzig, Leipzig, Germany
[2]now at: PIER-ELECTRONIC GmbH, Nassaustr. 33-35, 65719 Hofheim-Wallau, Germany
[3]Institute of Environmental Physics, University of Bremen, Bremen, Germany

Correspondence to: A. Ehrlich
(a.ehrlich@uni-leipzig.de)

1 Introduction

The comments of the reviewer have been helpful to improve the manuscript. Especially the question on the dependence of solar zenith angle on the retrieval results and the missing comparison with in situ measurements provided more understanding of the retrieval algorithm and of the radiative effects between clouds and surface.

The detailed replies on the reviewers comments are given below.

The reviewers comments are given bold while our replies are written in regular roman letters. Citations from the revised manuscript are given as indented and italic text.

Detailed Replies

1. The authors used the solar zenith angle of 63° to describe the dependence of the retrieval of cloud optical properties on snow surface albedo grain size. A note on how it would change with a different solar zenith angle would be useful for completeness. His note would also be useful in section 4.2.

The solar zenith angle of 63° was used because of the two case studies presented in the manuscript. We now did rerun the sensitivity study for solar zenith angles of 45° and 80°. It was found that the uncertainties in retrieved τ due to a wrong assumption of the grain size do not significantly change with solar zenith angle. However, for low Sun, $\theta = 80°$, the bias in retrieved $r_{\mathrm{eff,C}}$ was slightly reduced, while for $\theta = 45°$, the uncertainties of the retrieved $r_{\mathrm{eff,C}}$ are increased (see Figure 1). This can be explained by the probability that photons interact with the surface. This is lower for high solar zenith angle. We added this general dependency on solar zenith angle to the revised manuscript:

> *The numbers presented here, were obtained for a solar zenith angle of $\theta_0 = 63°$. For simulations with different solar zenith angles, similar grain size effects are observed. In general, the magnitude of the grain size effect of τ does not significantly change with θ_0. However, for low Sun, large θ_0, the grain size effect on the retrieved $r_{\mathrm{eff,C}}$ was slightly reduced, while for higher Sun, small θ_0, the effects increase. This is caused by the increased probability that radiation interacts with the surface in case of decreasing solar zenith angle.*

The snow grain size effect on retrieved τ does not depend on the solar zenith angle, while the effect on $r_{\mathrm{eff,C}}$ is larger for a higher Sun.

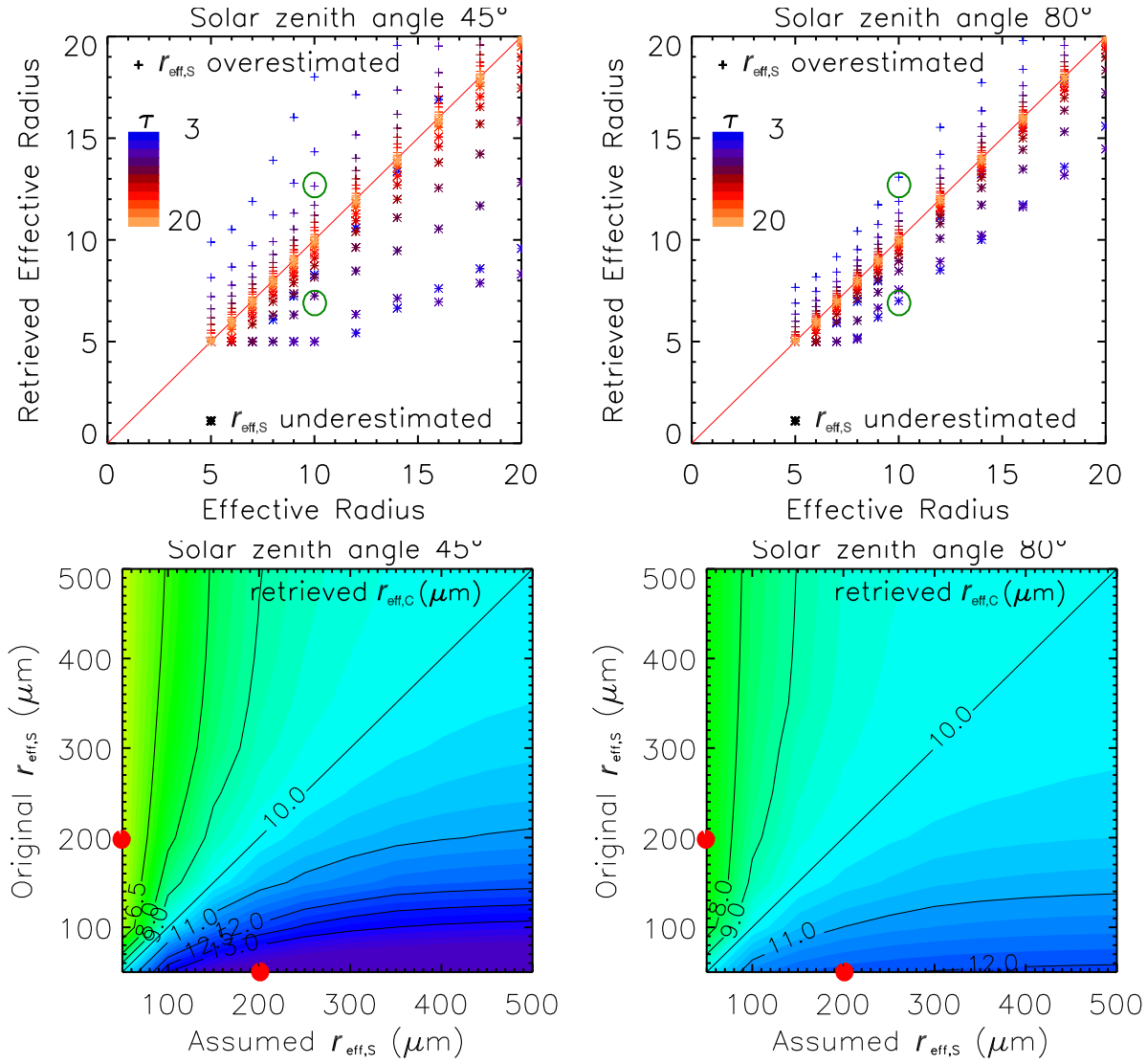

Figure 1. Comparison of retrieval uncertainties for solar zenith angle of 45° (left panels) and 80° (right panels). Upper plots show the comparison of synthetically retrieved $r_{\mathrm{eff,C}}$ with the original parameter value. Calculations in the upper panels are performed for assuming a larger snow effective grain size of $r_{\mathrm{eff,S}} = 200\,\mu\mathrm{m}$ instead of the original $r_{\mathrm{eff,S}} = 50\,\mu\mathrm{m}$ (crosses) and a smaller snow effective grain size of $r_{\mathrm{eff,S}} = 50\,\mu\mathrm{m}$ instead of the original $r_{\mathrm{eff,S}} = 200\,\mu\mathrm{m}$ (asterisks). In the lower panels all combinations of assumed and original $r_{\mathrm{eff,S}}$ are analyzed for a specific cloud of $\tau = 4$ and $r_{\mathrm{eff,C}} = 10\,\mu\mathrm{m}$.

Additionally, we used the new simulations to estimate the sensitivities of the spectral reflectivity to the three cloud and snow parameter for different solar zenith angles. Not significant differences were found in the spectral separation of the sensitivities. Figures 3 and 1 show the calculated standard deviations and principle component weighting for solar zenith angle of 45° and 80°. The wavelength dependent sensitivities of the cloud reflectivities did change only minor still allowing a separation of the three parameters by measurements at different wavelengths. Similarly, the retrieval grid of the forward simulations was only shifted to one or another direction. The orthogonality and potential ambiguities are almost unchanged. In the revised manuscript we added:

The results are presented for a solar zenith angle of $\theta_0 = 63°$ but are applicable to larger and smaller θ_0.

Although the retrieval was applied to cases with a specific solar zenith angle only, radiative transfer simulations showed that the spectral sensitivities used in the retrieval algorithm are similar in case of smaller or larger solar zenith angles.

2. Section 2.2 is slightly difficult to follow, please refine descriptions.

We reordered some passages in order to improve the readability. See marked up manuscript for all changes.

3. The use of percentages to denote uncertainty is slightly ambiguous and should be better defined.

Yes, we agree, percentages can be difficult to interpret. Therefore, we added how the percentage have to be read. In addition, the correct values are always given when percentages are used.

... the snow grain size effect, expressed by the percentage deviation of the retrieved from the original true value, ...

4. The use of the mean standard deviation per respect to a variable seems to be quite novel. Maybe more description is needed, especially to address the possible covariability of some parameters (i.e. sigma_tau is most variable when there is a high reff_c).

The mean standard deviation was used to provide an efficient way to identify wavelengths that are sensitive to a single cloud or snow parameter. Therefore, we aimed to include all simulations. E.g., for each cloud, a standard deviation of all simulations with different $r_{\mathrm{eff,S}}$ was calculated. $\sigma_{r_{\mathrm{eff,S}}}$ is then derived by averaging these standard deviations for all different clouds. It is right, that for a selection of the set of simulated clouds or snow grain sizes different numbers might be obtained. With the intention to provide a simple retrieval algorithm based on measurements at three wavelength, we did not extended this analysis into more detail. In addition, we finally selected wavelengths corresponding to MODIS bands. A limitation to only a few spectral band will limit the results of a more detailed study investigating the spectral sensitivities for different sub-samples of cloud and snow parameters. To point the use of the mean standard deviations more clearly we added the following sentences in the manuscript.

E.g., for each cloud, a standard deviation of all simulations with different $r_{\mathrm{eff,S}}$ was calculated. $\sigma_{r_{\mathrm{eff,S}}}$ is then derived by averaging these standard deviations for all different clouds.

Similarly, the use of sub samples of the full cloud and snow parameter range investigated here might change the derived values.

5. Description of the identification process of when the retrieval of snow grain size and cloud property fails would be a useful addition to this paper.

In the manuscript, we mentioned, that the retrieval may fail if mixed-phase clouds are present. In that case "fail" does not mean, that the algorithm may stop at some step and does not provide a results. "Fail" refers to wrong results which may be far off the real snow or cloud properties. For mixed-phase clouds, also the cloud ice crystals will absorb the solar radiation at similar wavelengths as snow; the spectral signatures of cloud and snow properties might be merged stronger than for liquid clouds. Therefore, the retrieved snow grain size might be biased by the cloud ice ($r_{\mathrm{eff,C}}$), and vice versa. Still the retrieval would provide a results but this might be wrong. To clarify this, we changed the manuscript to:

In this case, the retrieval may provide unrealistic cloud properties as the ice crystals absorb solar radiation at similar wavelengths as the snow surface does.

6. The retrieval is applied to data over land although no mention of that in the description of the retrieval methodology description.

Yes, for Case I, the retrieval was also applied for snow covered land surface. These data are only presented in the maps of Figure 8. The time series in Figure 6 does not include the full flight track, as mentioned in the manuscript. However, the application of the retrieval to land surfaces of sufficient snow cover is justified, as the surface below a snow layer does not effect the snow albedo, when the snow layer exceeds a thickness of about 10 cm or more. In the revised manuscript we added a note, that the retrieval was also applied to snow covered land surfaces.

Note that here a longer time series is shown than presented in Figure 6. This includes areas with snow covered land surfaces, for which the retrieval can be applied assuming that the snow layer is sufficiently thick and the snow albedo is not affected by the underlying surface (Warren, 2013)

7. A note on the availability of surface or in situ measurements for the 2 cases would be helpful.

Measurements of snow grain size on the sea ice have not been conducted during the campaign. Therefore, no reference is available. However, airborne cloud microphysical measurements have been obtained during the flight. Having only one aircraft, Polar 5, the in situ and remote sensing measurements had to be performed subsequently. For both investigated examples, Case I and II, the remote sensing flight legs were flown first. About one hour later the in situ measurements were obtained on the same flight leg. These measurements were included in the revised manuscript and compared to the retrieval results. The following sections have been added:

Cloud microphysical in situ measurements on board of Polar 5 were use to validate the retrieved $r_{\mathrm{eff,C}}$d. A Cloud Droplet Probe (CDP) provided size resolved cloud particle concentrations in the size range from 2.5 μm to 46 μm and

corresponding $r_{\mathrm{eff,C}}$ (Klingebiel et al, 2015). Using only one aircraft, the in situ and remote sensing measurements had been performed subsequently. For both investigated Cases I and II, the remote sensing flight legs were flown first. Roughly one hour later the in situ measurements were obtained at the same location following the flight track of the remote sensing sequence. Due to the stable meteorological conditions, changes of the cloud properties with time are expected to be small which allows a comparison of in situ and remote sensing data. A reference to validate the retrieved snow grain size is not available because no ground-based measurements on the sea ice have been conducted during VERDI.

In situ cloud microphysical measurements of $r_{\mathrm{eff,C}}$ had been obtained along the same flight track about one hour after the remote sensing measurements. At cloud top, two derived vertical profiles show $r_{\mathrm{eff,C}}$ between 6 μm and 7.5 μm, which is in the range of the retrieval results.

The in situ microphysical measurements cover two cloud profiles along the same flight track, one observed above open ocean and one above sea ice. Both profiles showed no difference with $r_{\mathrm{eff,C}}$ of about 9 μm at cloud top, which are higher compared to Case I and in agreement with the retrieval results.

8. The conclusion is well written, especially with the inclusion of the bullet points.

Thanks!

9. P.2 line 33, exact meaning of sentence not clear, please define what is an improvement of uncertainty by 20%, is it an uncertainty range that is 20% less, or that is it 20% smaller compared to the retrieved value.

Yes, by using "improve by 20 %" the meaning was not sufficiently clear. Indeed, Rolland and Liou (2001) calculated the percentage reduction the the uncertainties range. The absolute reduction differs for different clouds. Therefore, the relative numbers are given. We rephrased the sentence to:

Rolland and Liou (2001) showed that the retrieval uncertainties of thin cirrus can be reduced by 20 % for optical thickness and by 45 % for ice crystal effective radius when a reasonable estimate of the surface albedo is applied.

10. Fig. 2 could be made clearer if the optical thickness and cloud particle effective radius were put directly on the figure. At least an indication of the low end of the optical thickness and effective radius would be needed.

We added such labels in the revised figure.

11. P.5 line 5, cloud reflectivity is also impacted at wavelengths lower than 1000 nm, the word 'only' is erroneous in this case, maybe use a less strict word.

Yes, "only" is not true. We changed the sentence to:

The simulations illustrate that τ impacts γ_λ primarily at wavelengths larger than $1000\,\mathrm{nm}$ where the snow albedo is lower than 0.8, while lower wavelengths are less sensitive to τ.

12. P.6 line 9, Sentence slightly difficult to follow.

That's true, the sentence was way to long. We split now and rephrased to:

> *For liquid water cloud retrievals obtained over snow surfaces with unknown grain size, the snow grain size effect on uncertainties of retrieval results was quantified. Therefore, synthetic measurements obtained from the retrieval forward simulations as introduced in Section 2.1 are applied. For each synthetic measurement defined by* τ*,* $r_{\mathrm{eff,C}}$*, and* $r_{\mathrm{eff,S}}$ *a set of retrieval assuming different values of effective snow grain sizes were performed.*

13. P.6 line 12 Please elaborate or define more clearly 'retrieval forward simulation'

The forward simulations of the retrieval are introduced in Section 2.1. We added this reference here.

> *Therefore, synthetic measurements obtained from the retrieval forward simulations as introduced in Section* **??** *are applied.*

14. P. 8 line 15, typo, should read 'In cases where liquid water clouds are...'

Has been corrected in the revised version.

15. Fig. 4 – consider only showing the absolute value of the PCA spectra, for easier comparison to the mean standard deviation values.

Yes, we already thought about that, but concluded that the sign of the PCA weightings should not be neglected as it is a valid information. On the other hand, the magnitude itself is important to compare the different principle components. Therefore, we adjusted the plot and showed only absolute values. Original negative weightings are plotted as dashed lines to indicate the sign. However, this new plot looks to busy and we think the main information is lost due to the different line styles. We therefore, would like to keep the original version, but included the alternative version here in the replies (Figure 2).

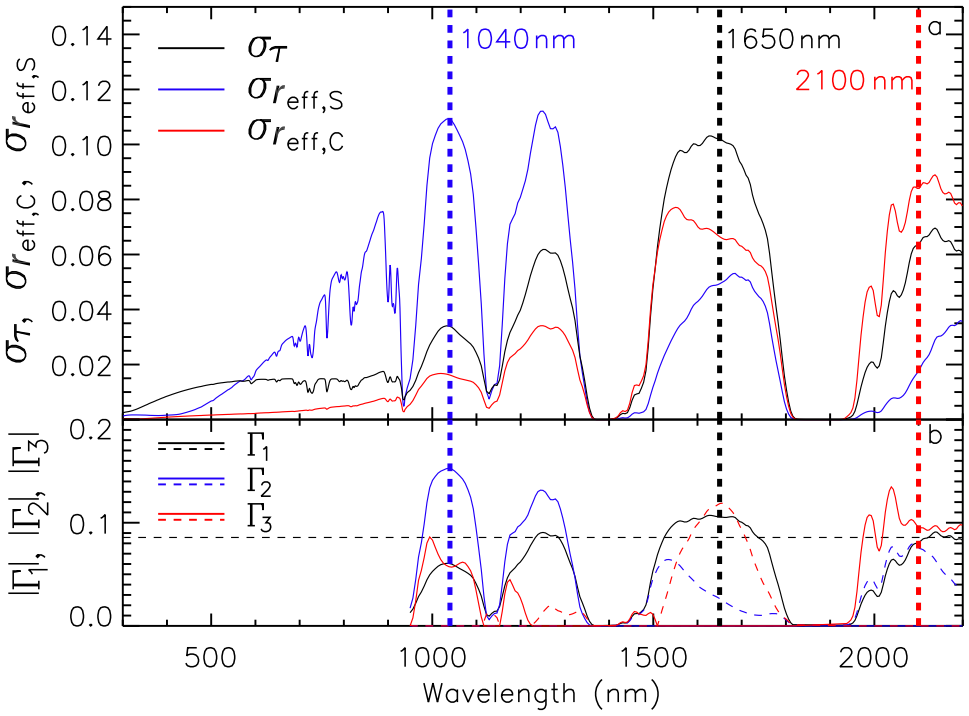

Figure 2. Mean standard deviations of spectral cloud reflectivity σ_τ, $\sigma_{r_{\mathrm{eff,C}}}$, and $\sigma_{r_{\mathrm{eff,S}}}$ with respect to a single cloud or snow parameter τ, $r_{\mathrm{eff,C}}$, and $r_{\mathrm{eff,S}}$ calculated for the sets of radiative transfer simulations (panel a). The absolute values of the first three spectral weights Γ_1, Γ_2, and Γ_3 of a principle component analysis are given in panel b. Dashed lines indicate negative values, solid lines positive values of Γ_1, Γ_2, and Γ_3.

16. Typo P.12, line 10, 'too weak' instead of 'to week', sentence would benefit from being more precise.

Has been corrected in the revised version.

17. Typo P.12, line 13 'ice floes' instead of 'ice flows'

Has been corrected in the revised version.

18. P.12, line 16, revise sentence for the use of the word 'also'

Has been corrected in the revised version to:

> *A surface with a high albedo always enhances the upward radiance above a cloud even in the case of optically thick clouds.*

19. Comment, Section 5, the radiometric uncertainties quoted for the ratios seem large considering the calibration uncertainty partially cancel.

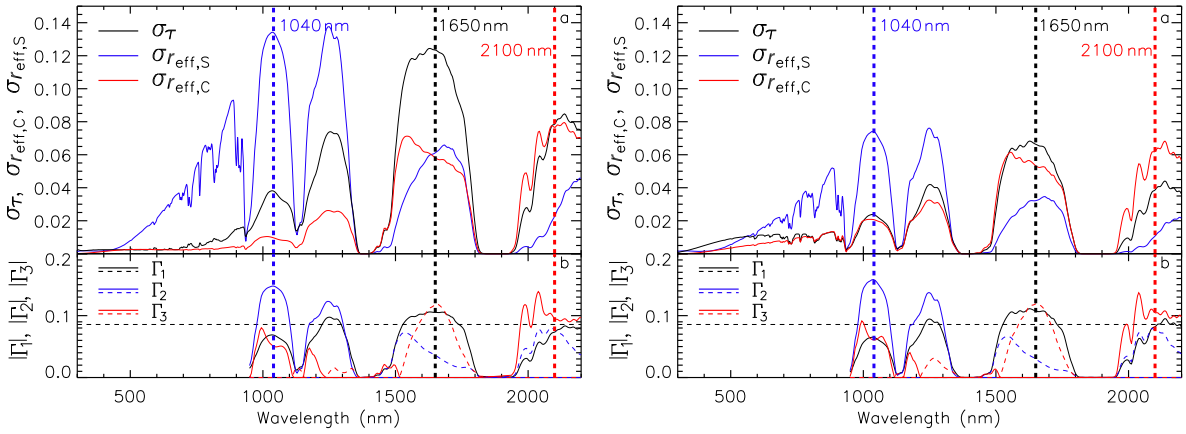

Figure 3. Same es Figure 2 but for solar zenith angle of 45° (left) and 80° (right)

We carefully calculated the uncertainties of the ratios by considering the uncertainties of the individual radiance measurements. Apart from the radiometric calibration which cancels out for the ratios, the largest contribution to the high uncertainties results form the signal to noise ratio. The noise and dark signal of the spectrometers differ between the two spectrometer types operated in SMART and also within the spectrometer spectral range. Especially the measurements at 2100 nm wavelength are almost at the end of the spectrometer photo diode array where the sensitivity strongly decreases. Therefore, the signal to noise ratio of R_3 is quite large. In addition, the radiance is lower at larger wavelengths and even lower in the absorption bands used for the retrieval. These low radiances reduce the signal to noise ratio compared to shorter wavelengths covered by the same spectrometer. This effect can easily lead to uncertainties ranging above 10%.

Reply on Anonymous Referee #2 (AMT-2017-50)

André Ehrlich[1], Eike Bierwirth[1,2], Larysa Istomina[3], and Manfred Wendisch[1]

[1]Leipzig Institute for Meteorology (LIM), University of Leipzig, Leipzig, Germany
[2]now at: PIER-ELECTRONIC GmbH, Nassaustr. 33-35, 65719 Hofheim-Wallau, Germany
[3]Institute of Environmental Physics, University of Bremen, Bremen, Germany

Correspondence to: A. Ehrlich
(a.ehrlich@uni-leipzig.de)

1 Introduction

The comments of the reviewer have been helpful to improve the manuscript. We are especially thankful for the plenty corrections of the text and punctation!

The detailed replies on the reviewers comments are given below.

The reviewers comments are given bold while our replies are written in regular roman letters. Citations from the revised manuscript are given as indented and italic text.

Detailed Replies

It carries the potential to be implemented for existing imagers (MODIS, VIIRS) which, for some reason, is not emphasized in the current version.

We agree that the proposed method could be implemented for MODIS or VIIRS. The reason why we did not highlighted this explicitly is that we think we would have to prove it when making this statement. In the revised version we carefully addressed the possibility to use the method for satellite imagers; once in the algorithm description and once in the conclusions.

> *Except for λ_1, all wavelengths that were chosen for the algorithm are covered by the satellite imagers MODIS and VIIRS. To apply the algorithm to global observations by these instruments, λ_1 can be exchanged by the 1240* nm *wavelength band where cloud reflectivity is still most sensitive to $r_{\mathrm{eff,S}}$.*

> *Therefore, the proposed retrieval method has some potential to be implemented for existing spaceborne imagers such as MODIS or VIIRS. Due to the limited number of spectral bands, for these two instrument λ_2 would have to be exchanged by the 1240* nm *wavelength band where cloud reflectivity is still most sensitive to $r_{\mathrm{eff,S}}$.*

1) The language, structure and grammar diminish the potential impact of the manuscript because it becomes hard to read as a result. In sections 4 and 5, it was obvious that it had not been fully proof-read, and it seemed premature to afford it a full review at this point in time. It is beyond the scope of a science review to highlight such issues, but a

few examples are listed below. It is in the interest of the authors to revise the language. In some sections (4 and 5 in particular), it could be shortened without losing its content.

We are sorry about the incorrect language and grammar. We revised the manuscript and tried to improve as much as possible. However, as we are no native speakers, we suggest to have a professional copy-editing by the journal. Languages changes in the text can be found in the highlighted manuscript version.

2) In general, the science seems sound. However, it is surprising that the retrieval characterization is done without invoking principles of general inverse theory. This is especially important because the retrieval grid is not orthogonal for the most part. This means that there is no 1:1 mapping from observations to retrieval parameters, as the authors clearly acknowledge. But why, then, is the error characterization and propagation done in a fairly "brute force" way as visualized in Figure 7? In the framework of optimal estimation, one could have arrived at a statistically defensible retrieval characterization on the basis of the a-posteriori co-variance while fully taking into account measurement and model uncertainties. That said, a less rigorous error analysis such as done here is acceptable for initial and exploratory studies, as long as it is categorized as such.

Yes, this is right! To fully understand the uncertainties of the retrieval other statistical methods would have been needed. However, the intention of our study was to illustrate the concept of such a tri-spectral retrieval that allows to combine cloud and snow optical properties. Therefore, we kept the uncertainty analysis simple, also because the retrieval was only applied to two selected cases of specific solar zenith angle and to the nadir viewing direction of the airborne measurements. A more detailed analysis should also take into account the different sensitivities for different viewing geometries. We therefore changed the manuscript at different locations in order to point out clearly, that the manuscript presents only a feasibility study to the method but not a fully developed and characterized retrieval algorithm. A detailed comprehensive uncertainty analysis is beyond the scope of this paper and can be part of studies where the method is applied to a more general data set.

> *In a feasibility study, spectral cloud reflectivity measurements collected by the Spectral Modular Airborne Radiation measurement sysTem (SMART) during the research campaign Vertical Distribution of Ice in Arctic Mixed-Phase Clouds (VERDI, April/May 2012) were used to test the retrieval procedure.*
>
> *In a feasibility study in Section 5, the algorithm that is limited to cases of liquid water clouds is applied to two specific cases,...*
>
> *The retrieval algorithm was tested in a feasibility study for airborne observations by SMART during VERDI in 2012.*
>
> *For this first application of the new tri-spectral retrieval algorithm, a rather simplistic analysis was applied. A more general understanding of the retrieval sensitivities and uncertainties can be achieved by optimal estimation techniques, which is beyond of the scope of this paper.*

*** It should be mentioned somewhere in the manuscript that this study is strictly valid only for snow-covered surfaces with sufficient geometric (and therefore optical) thickness of the snow. The reference to Malinka (2016) is a bit mis-**

leading because it sounds as though white ice could be still be represented as snow. This is in stark contrast to multiple publications by, e.g., Perovich for such cases. They show a distinct spectral dependence in the visible wavelength range, and albedos well below 1.

We are aware that snow and white ice albedo are different at visible wavelengths. But there are reasons why the retrieval approach is still applicable, with larger uncertainties, to white ice or a mixtures of sea ice, open leads or melt ponds. In this cases still more accurate cloud properties compared to methods assuming a fixed snow/sea ice albedo can be derived, because the tri-spectral retrieval considers the change of the spectral albedo at the three wavelengths.

1) Visible wavelengths where white ice albedo and snow albedo have different spectral signatures are not used in the proposed retrieval. At larger wavelengths, where mostly the absorption by ice and not the scattering processes are relevant, the spectral pattern of white ice albedo, which is not water saturated, i.e. dry white ice, is similar to a snow albedo. Therefore, also the snow albedo model used in our retrieval approach can be applied to approximate the albedo of white ice in these spectral ranges. But of course not in the visible part of the solar spectrum. More sophisticated albedo models such as by Malinka et al. (2016) have to be used to construct the full spectral albedo. But then either measurements at visible wavelengths have to be included or information on the effective optical thickness are needed. In the revised manuscript we corrected:

> *Additionally, at wavelengths larger than 1000* nm *the albedo of white sea ice that is not covered by snow and not water saturated, i.e. dry white ice, is lower than that of snow-covered sea ice and, therefore, can be characterized by larger effective snow grain sizes (Malinka et al., 2016).*

2) The retrieval does not provide a retrieval of the full spectral surface albedo. The aim is to retrieve a parameter, the effective snow grain size $r_{\mathrm{eff,S}}$, which determines the surface albedo in the applied snow albedo model. Of course, we can not reconstruct the albedo of sea ice in the full solar spectral range as the snow albedo model does not capture this. Using three wavelengths, only information at these wavelengths are available. Therefore, we can only say that a certain snow albedo model fits best to the measurements at these wavelengths. The snow albedo model used in the algorithm is based only on one parameter, the effective grain size. In this sense, the effective snow grain size is only a parameter defining the most likely surface albedo at the applied wavelengths. That's why we always name it "effective". Considering the "effective" character of $r_{\mathrm{eff,S}}$, also the albedo of white ice can be parameterized using $r_{\mathrm{eff,S}}$ (see 1).

3.) Other common satellite grain size retrievals that are only applied in clear sky condition, such as mentioned and presented in the study, do consider similar snow albedo models that are based only on the effective grain size $r_{\mathrm{eff,S}}$.

4.) However, to avoid larger uncertainties by white sea ice, the cases presented in the manuscript are carefully selected and are dominated by snow-covered sea ice. We highlighted this in the revised manuscript at different positions. E.g.:

> *..., observations have been selected where the surface conditions are close to the required pure snow surface.*
>
> *Photographs on a flight section in the same area below the clouds showed that the fast ice was partly free of snow, which may have caused the higher variability and the single peak of* $r_{\mathrm{eff,S}} = 300\,\mu\mathrm{m}$

However, the spectral signature of white sea ice and melt-pond-covered sea is close to the spectral albedo of pure snow for the wavelengths used in the retrieval. In that case, the retrieved $r_{\mathrm{eff,S}}$ is interpreted as an effective snow grain size representing an arbitrary surface albedo (white sea ice or melt ponds) with the same spectral characteristics above 1000 nm wavelength as a snow surface with $r_{\mathrm{eff,S}}$.

Furthermore, "white" ice is not explained. What other ice types are there that might be relevant for cloud remote sensing? A wider literature overview may be helpful.

Of course also other sea ice types are relevant for cloud remote sensing. Unfortunately, the proposed retrieval algorithm is not capable of considering these, e.g., blue ice, because of the different spectral albedo. Therefore, the algorithm is proposed for snow-covered surfaces. The only exceptions is the dry white ice, because it approximately can be treated similar to snow of large grains at wavelengths larger $1000\,\mathrm{nm}$. We therefore, do not want to include the definition of other ice types because this might be misleading and give the impression that the retrieval might be also working for such surfaces. Which is not the case. For "white ice" a reference is given in the introduction.

*** p5, L5-11. The reflectance at 1600 nm and 2100 both depend on optical thickness and effective radius; it is simply wrong to decouple them. Figure 2 clearly shows the non-orthogonality of such a lookup table.**

We did not state that both parameters are decoupled. We explicitly state on Page 6, Lines 5-7 that "... the reflectivities at both wavelengths are coupled to both cloud parameters.". Our only idea why the reviewers made this comment is that the sentence Page 5, Lines 9-11 lead to the impression, that the parameters are only linked to one wavelength. This sentence was used to describe the general idea of an bi-spectral cloud retrieval, were the different dependencies are utilized to derive cloud optical thickness and effective radius. To avoid the misinterpretation of this sentence, we rephrased:

The retrieval uses the different dependencies of $\gamma_{1600\,\mathrm{nm}}$ (less-absorbing wavelength) and $\gamma_{2100\,\mathrm{nm}}$ (high-absorbing wavelength) on cloud optical thickness and cloud droplet effective radius and basically follows the method by **?**.

*** Figure 3a/b are nice visuals of the main direction of this paper; perhaps this could be emphasized more.**

To emphasize the major results shown in these plots, we added in the abstract the following conclusions:

he impact of uncertainties of $r_{\mathrm{eff,S}}$ is largest for small snow grain sizes. While the uncertainties of retrieved τ are independent of the cloud optical thickness and solar zenith angle, the bias of retrieved $r_{\mathrm{eff,C}}$ increases for optically thin clouds and high Sun.

*** p8: The "standard deviation" and the "PCA" method are insufficiently explain. What is the data set that these methods operate on? Also, the PCA components don't necessarily have to map to a physical parameter as the manuscript seems to suggest.**

The data set used for these calculations was given in the first sentence of the section. In the revised manuscript, we more clearly described the use of the mean standard deviations to subsets of the simulations by adding the following sentences in the manuscript.

> *E.g., for each cloud, a standard deviation of all simulations with different $r_{\mathrm{eff,S}}$ was calculated. $\sigma_{r_{\mathrm{eff,S}}}$ is then derived by averaging these standard deviations for all different clouds.*
>
> *Similarly, the use of sub samples of the full cloud and snow parameter range investigated here might change the derived values.*

For the PCA it was already stated that we "... applied to the full set of simulations". It is true, that the weightings of the PCA do not necessarily have to map a single physical parameter. But obviously for the set of simulations presented in the manuscript this is the case. To avoid the impression, that this separation is given by theory, we changed the following sentence to:

> *Corresponding to the cloud and snow parameters changed in the simulations, the spectral weights Γ_1, Γ_2, and Γ_3 of the first three principle components are found to be associated with τ (Γ_1), $r_{\mathrm{eff,C}}$ (Γ_2), and $r_{\mathrm{eff,S}}$ (Γ_3).*

*** p10, L10: Using 860 nm as a reference wavelength for the first ratio is probably a bad idea unless the paper specifically limits itself to snow (rather than including ice). This is because (as stated above, and described by Perovich) ice has a distinct spectral shape and albedo magnitude at wavelengths below 1000 nm.**

Yes, for the current version we would like to limit the retrieval to snow covered surfaces and not extend it to other sea ice types. We first would like to illustrate the main idea that information of the surface albedo is still imprinted in spectral radiance measurements above clouds. Therefore, we prefer using measurements at 860 nm because at this wavelength the differences in snow and sea ice albedo is low. Of course, this similarity is completely gone once the sea ice starts melting or its surface gets water saturated. However, dry white ice with some scattering layer on top (of typically granular crystals) is comparable to the snow with not too fine grains. The publication by Malinka et al. (2016) states this exact point.

Also snow impurities do affect the spectral albedo less at 860 nm compared to shorter wavelengths. It is possible, that our approach can be extended to shorter wavelengths in order to detect a drop in the surface albedo at visible wavelengths related to different ice types. But therefore, we would need to use a more detailed snow/sea ice albedo model which is beyond the scope of this study.

*** p10, Table 1: This table is reminiscent of a covariance matrix. Why were these relationships not exploited in the framework of optimal estimation? What is the inverse theory foundation of this work?**

For us, the main intention of this study is to present the feasibility of retrieving cloud and snow properties simultaneously by making use of the spectral information that is provided by spectral measurements of cloud reflectivity. Therefore, we did not set the focus of our attention on the inverse theory but applied rather simple methods; spectral standard deviation and principle component analysis to identify sensitive spectral regions; propagation of normally distributed uncertainties through the retrieval to derive retrieved parameters with uncertainty estimate. As the sensitivities seems sound and the retrieval algorithm already provides reasonable results, we did not put more effort in improving the inverse method at this stage. Therefore, we now

pointed out more clearly that the study should be seen as a feasibility study. Later, more detailed analysis of sensitivities and uncertainties may follow. For changes in the manuscript see answer to comment number 2).

Grammar/English:

Thanks a lot for identifying all these mistakes. We are sorry, that these were not found by ourself and collecting all increased your work. We corrected all and tried our best to eliminate other incorrect grammar and typos.

Combined retrieval of Arctic liquid water cloud and surface snow properties using airborne spectral solar remote sensing

André Ehrlich[1], Eike Bierwirth[1,2], Larysa Istomina[3], and Manfred Wendisch[1]

[1]Leipzig Institute for Meteorology (LIM), University of Leipzig, Leipzig, Germany
[2]now at: PIER-ELECTRONIC GmbH, Nassaustr. 33-35, 65719 Hofheim-Wallau, Germany
[3]Institute of Environmental Physics, University of Bremen, Bremen, Germany

Correspondence to: André Ehrlich (a.ehrlich@uni-leipzig.de)

Abstract. ~~In the Arctic, the~~ The passive solar remote sensing of cloud properties over highly reflecting ground is challenging, mostly due to the low contrast between the ~~clouds and~~ cloud reflectivity and that of the underlying surfaces (sea ice and snow). Uncertainties in the retrieved cloud optical thickness τ and cloud droplet effective radius $r_{\mathrm{eff,C}}$ may arise from uncertainties in the assumed spectral surface albedo, which is mainly determined by the ~~commonly unknown snow effective~~ generally unknown effective snow grain size $r_{\mathrm{eff,S}}$. Therefore, in a first step ~~this~~ the effects of the assumed snow grain size ~~effect is quantified systematically for a~~ are systematically quantified for the conventional bi-spectral retrieval technique of τ and $r_{\mathrm{eff,C}}$ for liquid water clouds. ~~The largest impact of~~ In general, the impact of uncertainties of $r_{\mathrm{eff,S}}$ ~~of up to~~ is largest for small snow grain sizes. While the uncertainties of retrieved τ are independent of the cloud optical thickness and solar zenith angle, the bias of retrieved $r_{\mathrm{eff,C}}$ increases for optically thin clouds and high Sun. The largest deviations between the retrieved and true original values are found with 83 % ~~on~~ for τ and 62 % ~~on~~ for $r_{\mathrm{eff,C}}$~~was found in case of small $r_{\mathrm{eff,S}}$ and optically thin clouds~~.

In the second part of the paper a retrieval method ~~is presented that simultaneously retrieves~~ that simultaneously derives all three parameters (τ, $r_{\mathrm{eff,C}}$, $r_{\mathrm{eff,S}}$) ~~in order to account~~ and, therefore, accounts for changes of the snow grain size ~~in the cloud retrieval algorithm. Spectral cloud reflectivities~~ is presented. Ratios of spectral cloud reflectivity measurements at the three ~~wavelength~~ wavelengths $\lambda_1 = 1040\,\mathrm{nm}$ (sensitive to $r_{\mathrm{eff,S}}$), $\lambda_2 = 1650\,\mathrm{nm}$ (sensitive to τ), and $\lambda_3 = 2100\,\mathrm{nm}$ (sensitive to $r_{\mathrm{eff,C}}$) ~~were normalized to reflectivity ratios and~~ are combined in a tri-spectral retrieval algorithm. ~~Measurements~~ In a feasibility study, spectral cloud reflectivity measurements collected by the Spectral Modular Airborne Radiation measurement sysTem (~~SMART-Albedometer~~SMART) during the research campaign Vertical Distribution of Ice in Arctic Mixed-Phase Clouds (VERDI, April/May 2012) were used to test the retrieval procedure. Two cases of observations above the Canadian Beaufort Sea, one with dense snow-covered sea ice and another with a distinct snow-covered sea ice edge ~~were~~ are analyzed. The retrieved values of τ, $r_{\mathrm{eff,C}}$, and $r_{\mathrm{eff,S}}$ ~~consistently represented the~~ show a continuous transition of cloud properties across ~~this transition from~~ snow-covered sea ice ~~to the~~ and open water and ~~were comparable to~~ are consistent with estimates based on satellite data. ~~Analysis showed,~~ It is shown that the uncertainties of the tri-spectral retrieval increase for high values of τ, and low $r_{\mathrm{eff,S}}$ ~~, but nevertheless allows a simultaneous retrieval of cloud and surface snow properties providing snow effective grain size estimates~~ but nevertheless allow to estimate the effective snow grain size in cloud-covered areas.

1 Introduction

During boreal winter, 15 % of the Earth's surface is covered by snow and sea ice (Vaughan et al., 2013), while clouds cover roughly two thirds of the globe (Boucher et al., 2013). Both ~~,~~snow and clouds considerably increase the reflected solar radiation at top of atmosphere ~~albedo~~ and, therefore, are ~~eminent~~ essential for determining the Earth's radiative energy budget. Changes in ice, snow, and cloud cover ~~indicate climate warming especially~~ are both the result and cause of climate warming in Arctic areas (Wendisch et al., 2017). However, while snow and sea ice ~~show a large~~ exhibit a considerable seasonal variation, clouds ~~may~~ usually vary on shorter time and smaller spatial scales. Therefore, continuous observations of cloud and snow properties are important. Commonly, satellite remote sensing ~~is used~~ techniques are applied to monitor the ~~most~~ relevant radiative properties of clouds and snow, such as cloud optical thickness~~and~~ , cloud droplet effective radius, snow cover~~and snow effective grain size~~ , effective snow grain size, and soot concentration ~~(e.g., Stephens and Kummerow, 2007; Platnick et al., 2017; Zege et al., 2011; Painter et al.~~ (e.g., Stephens and Kummerow, 2007; Painter et al., 2009; Zege et al., 2011; Platnick et al., 2017).

In polar regions clouds cover large areas of snow, glaciers, and sea ice, which complicates the retrieval of ~~snow and cloud~~ their properties because the contrast between these bright surfaces and the clouds is low. At wavelengths typically used to retrieve cloud properties from solar spectral ~~reflectance~~ reflectivity measurements, the optical properties of clouds and snow are similar. Therefore, cloud retrieval algorithms utilize observations at wavelengths larger than 1000 nm where the snow albedo ~~becomes~~ is lower. Measurements at 1500 nm wavelength, where snow strongly absorbs solar radiation, were used by Krijger et al. (2011) and Gao et al. (1998) to improve the cloud detection above snow surfaces. Furthermore, cloud optical thickness and droplet effective radius were successfully retrieved above snow surfaces by ~~changing the~~ selecting a channel combination of the retrieval algorithm ~~of the~~ in the near infrared spectral region. E.g., the 1640 nm and 2130 nm band combination was used for the Moderate Resolution Imaging Spectroradiometer (MODIS)~~to the 1640~~, while the 1240 nm ~~and 2130~~band was applied instead of the 672 nm band ~~combination (Platnick, 2001; King et al., 2004)~~for the Visible Infrared Imaging Radiometer Suite (VIIRS) (Platnick, 2001; King et al., 2004; Platnick et al., 2013).

However, the cloud reflectivity in this spectral range is also affected by changes of the spectral albedo of the snow surface (Wiscombe and Warren, 1980). The smaller the snow grains, the higher the surface albedo ~~becomes~~ and the more radiation is reflected by the surface. Therefore, ~~retrieving~~ the retrieval of cloud properties (optical thickness and droplet effective radius) over snow surfaces requires a precise assumption on the ~~snow effective~~ effective snow grain size below the clouds. Snow grain size ~~may vary~~ varies temporally and spatially due to ~~new~~ precipitation that reduces~~the snow grain size~~ , and because of the snow metamorphism that slowly increases the snow grain size (e.g., Flanner and Zender, 2006; Jacobi et al., 2010). In polar areas, the ~~snow effective~~ effective snow grain size typically ranges between 50 µm for freshly fallen snow and 1000 µm for aged snow (Wiebe et al., 2013). This snow metamorphism changes the broadband surface albedo by 14 % from 0.89 to 0.77. ~~The majority of this change~~ Most of this effect on albedo occurs at longer wavelengths where the imaginary part of the refractive index of ice is high. ~~Therefor~~Therefore, the decrease of the spectral albedo at 1300 nm is enhanced to 65 % from 0.75 to 0.26 (Dang et al., 2016). In mid-latitude areas the snow metamorphism is often accelerated ~~due to higher temperaturesand may lead to snow effective grain sizes~~ by higher temperatures, which can lead to effective snow grain sizes of up to 3000 µm ~~and~~ causing an

even stronger reduction of snow albedo (Singh, 2001; Derksen et al., 2014). Additionally, at wavelengths larger than 1000 nm the albedo of white sea ice that is not covered by snow ~~is reduced compared to~~ and not water saturated, i.e. dry white ice, is lower than that of snow-covered sea ice and, therefore, can be characterized by larger ~~snow effective~~ effective snow grain sizes (Malinka et al., 2016). However, most cloud ~~retrievals~~ retrieval techniques do not consider ~~such~~ for a variation of the snow and sea ice albedo. For the MODIS cloud product Collection 6~~only~~ , a fixed surface albedo of 0.03 for both wavelength bands (1640 nm and 2130 nm) is assumed over sea ice or snow-covered areas (King et al., 2004). ~~Different~~ In contrast to land surfaces, no spatial or temporal changes of the snow and sea ice albedo are considered.

Uncertainties of the surface albedo ~~can significantly~~ affect the retrieval of cloud optical properties~~(e.g., Fricke et al., 2014; Rolland and Lio~~ ~~. Most of these~~ , which has been shown by Rolland and Liou (2001), Platnick (2001), and Fricke et al. (2014). These studies focus on optically thin clouds over typical land surfaces with a high variability of the spectral albedo ~~for~~ at wavelengths below 1 µm. For ~~a~~ an optically thin cirrus, Fricke et al. (2014) estimated retrieval uncertainties of up to 50 % for the ice crystal effective radius depending on cloud optical thickness. Rolland and Liou (2001) showed that the retrieval uncertainties of thin cirrus can be ~~improved~~ reduced by 20 % for optical thickness and by 45 % for ice crystal effective radius when ~~an improved~~ a reasonable estimate of the surface albedo ~~variability~~ is applied. For snow-covered areas, only the difference between ~~sea ice and ice free albedo~~ snow/sea ice albedo and the albedo of the sea ice free ocean has been addressed ~~and considered~~ in improved retrieval algorithms (Platnick, 2001). ~~An estimate of how changes of the snow albedo effect cloud retrieval is missing~~ So far, no estimates of the effect of a varying snow albedo on cloud retrievals have been reported in the literature~~so far~~.

For satellite observations of spectral solar radiation, retrieval algorithms that provide ~~snow effective~~ effective snow grain size have been developed by ~~Zege et al. (2011); Painter et al. (2009)~~Painter et al. (2009) and Zege et al. (2011). These techniques ~~utilize~~ exploit the dependence of spectral snow albedo ~~/reflectivity on the snow effective~~ and reflectivity and effective snow grain size. A larger ~~snow effective~~ effective snow grain size increases the photon path length within the snow grain and hence the probability that radiation is absorbed in the snow layer~~which would~~ , which reduces the snow albedo. As already thin snow layers ~~determine~~ dominates the radiation reflection by the surface, the retrievals are most sensitive to the uppermost snow layer and~~cover~~ , thus, changes by precipitation~~and snow metamorphism(Wiebe et al., 2013; Libois et al., 2013). In addition, the retrieval algorithms by Zege et al. (2011) and Painter et al. (2009)~~ , snow metamorphism, and the concentration of impurities are of utmost importance (Wiebe et al., 2013; Libois et al., 2013). The retrieval methods by Painter et al. (2009) and Zege et al. (2011) use these sensitivities and estimate the black carbon concentration in the snow~~surface that mostly effects~~ , which mostly affects the visible range of the spectral albedo. Unfortunately, these satellite retrievals of snow properties ~~may~~ do not cover the full spatial and temporal evolution of ~~snow effective~~ effective snow grain size and snow albedo as they are limited to cloud free areas (Lyapustin et al., 2009; Zege et al., 2011). However, ~~especially~~ cloud layers in polar regions ~~cloud layers that~~ are often observed to prevail for several days ~~are frequently observed~~ (Herman and Goody, 1976; Shupe et al., 2006, 2011). In ~~that case~~such a case, the cloud retrieval may suffer from an outdated assumption on snow or sea ice albedo. A correct solution is only possible ~~,~~ if snow and cloud properties are determined in combination as suggested in this paper.

Measurements of spectral cloud reflectivity have been successfully applied to distinguish between liquid and ice water clouds (Pilewskie and Twomey, 1987; Ehrlich et al., 2008; LeBlanc et al., 2015). Making use of differences in the spectral absorption

of liquid water and ice, which are manifested in the spectral shape of the cloud reflectivity~~can be analyzed to determine different~~ , several indices to identify the dominant cloud phase are defined. Similarly, this study makes use of the different spectral absorption characteristics for snow surfaces and liquid water clouds to ~~develop a method that allows to~~ retrieve cloud and snow properties ~~simultaneous~~simultaneously. To illustrate the need of such retrieval methods ~~, in Section 2~~ the uncertainties due to uncertainties in the assumed snow albedo on the retrieval of cloud properties will be quantified in Section 2. The new retrieval method will be introduced in Sections 3 and 4 including the identification of ~~suited~~ most suitable wavelengths applied in the retrieval ~~and~~ as well as the forward simulations of cloud reflectivity~~that build the backbone of the retrieval. In~~ . In a feasibility study in Section 5, the algorithm that is limited to cases of liquid water clouds is applied to two specific cases, which have been observed by airborne spectral cloud reflectivity measurements during the field campaign Vertical Distribution of Ice in Arctic Clouds (VERDI) over the Canadian Beaufort Sea in 2012.

2 Uncertainties of bi-spectral cloud retrieval over snow

2.1 Forward simulations

Based on radiative transfer simulations the impact of uncertainties of the snow albedo on the retrieved cloud properties is quantified. The spectral solar ~~radiation~~ reflectivity above a liquid water cloud layer was simulated using the DISORT 2 radiative transfer solver embedded in the library for radiative transfer (libRadtran, Emde et al., 2016). A solar zenith angle of 63° representative for Arctic conditions around spring was chosen in the simulations. Typical Arctic boundary layer liquid water clouds located between 200 m and 500 m altitude were ~~simulated~~assumed. Cloud optical thickness τ was varied from 1 to 20; cloud droplet effective radius $r_{\mathrm{eff,C}}$ between 2 µm and 25 µm. For all clouds, simulations with different surface albedo covering ~~snow effective~~ effective snow grain sizes $r_{\mathrm{eff,S}}$ between 10 µm and 800 µm were performed. The spectral snow albedo ρ_λ was calculated with the parametrization by Zege et al. (2011) using the refractive index of ice ~~presented~~ by Warren and Brandt (2008) and a form-factor $A = 5.8$. This form factor is adopted from Zege et al. (2011) and accounts for the non-sphericity of snow grains; it represents a mixture of randomly oriented hexagonal plates and columns with rough surfaces. This mixture and, therefore, the form-factor A may ~~differ in reality~~ vary depending on the local snow properties. However, an uncertainty of A can be attributed to an uncertainty in the effective snow grain size as both properties have the same spectral impact on the snow reflection characteristics, such as spectral albedo. Snow impurities by black carbon were neglected as the absorption by black carbon is typically limited to wavelengths less than 1000 nm (e.g., Warren and Wiscombe, 1980; Liou et al., 2014) that are not used in cloud retrieval over snow surfaces. A set of calculated spectral snow albedo ρ_λ is presented in Figure 1a, which illustrates the decrease of ρ_λ with increasing values of $r_{\mathrm{eff,S}}$ for wavelengths $\lambda > 1000$ nm where the imaginary part of the refractive index of ice is high (Figure 1c).

The simulated upward nadir radiance I_λ and downward irradiance F_λ were converted into spectral cloud reflectivity γ_λ defined by,

$$\gamma_\lambda = \frac{\pi \cdot I_\lambda}{F_\lambda}. \quad (1)$$

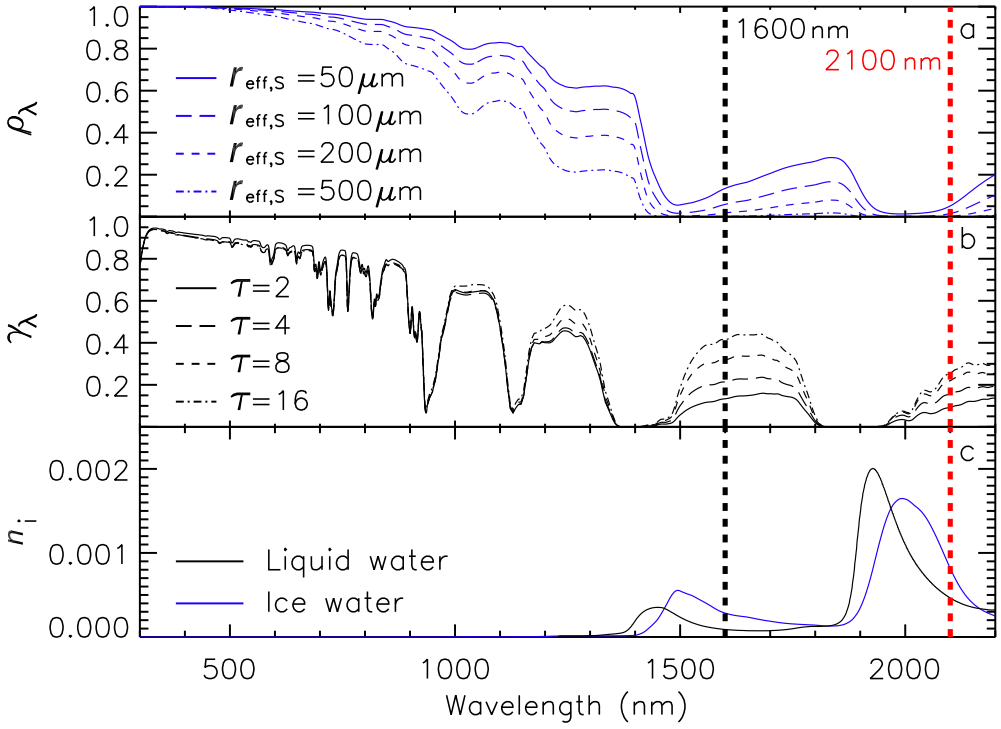

Figure 1. Comparison of spectral snow albedo ρ_λ (a) and cloud reflectivity γ_λ (b) for different $r_{\mathrm{eff,S}}$ and τ, respectively. Clouds reflectivity has been simulated for clouds with $r_{\mathrm{eff,C}} = 10\,\mu\mathrm{m}$ that are located above a snow surface with $r_{\mathrm{eff,S}} = 100\,\mu\mathrm{m}$. The imaginary part of the refractive index of ice and liquid water is given in panel (c). Vertical lines indicate the wavelength used in the bi-spectral cloud retrieval.

In Figure 1b a set of γ_λ for typical values of τ between 2 and 16 is shown for a fixed cloud effective droplet size of $r_{\mathrm{eff,C}} = 10\,\mu\mathrm{m}$ and a typical ~~snow effective~~ effective snow grain size of $r_{\mathrm{eff,S}} = 100\,\mu\mathrm{m}$. The simulations illustrate that τ impacts γ_λ ~~only at wavelengths $\lambda > 1000$~~primarily at wavelengths larger than 1000 nm where the snow albedo is lower than 0.8, while lower wavelengths are less sensitive to τ.

Based on the simulated cloud reflectivities, which are used as synthetic measurements, ~~a~~ the commonly used bi-spectral cloud retrieval algorithm was applied to obtain cloud optical thickness and droplet effective radius. This retrieval method is similar to the cloud product of MODIS (Platnick, 2001). The retrieval uses the ~~dependence~~ different dependencies of $\gamma_{1600\,\mathrm{nm}}$ (less-absorbing wavelength) ~~to cloud optical thickness and the dependence of~~ and $\gamma_{2100\,\mathrm{nm}}$ (high-absorbing wavelength) ~~to cloud~~ on cloud optical thickness and cloud droplet effective radius and basically follows the method by Nakajima and King (1990).

The bi-spectral retrieval grid obtained from the simulated cloud reflectivities is presented in Figure 2 for three ~~snow effective~~ effective snow grain sizes: 50, 100, and 500 µm. The grids significantly differ and show a considerable snow grain size effect especially for low values of $\gamma_{1600\,\mathrm{nm}}$, while at higher reflectivities the grids tend to converge. The reflectivity $\gamma_{2100\,\mathrm{nm}}$ is less

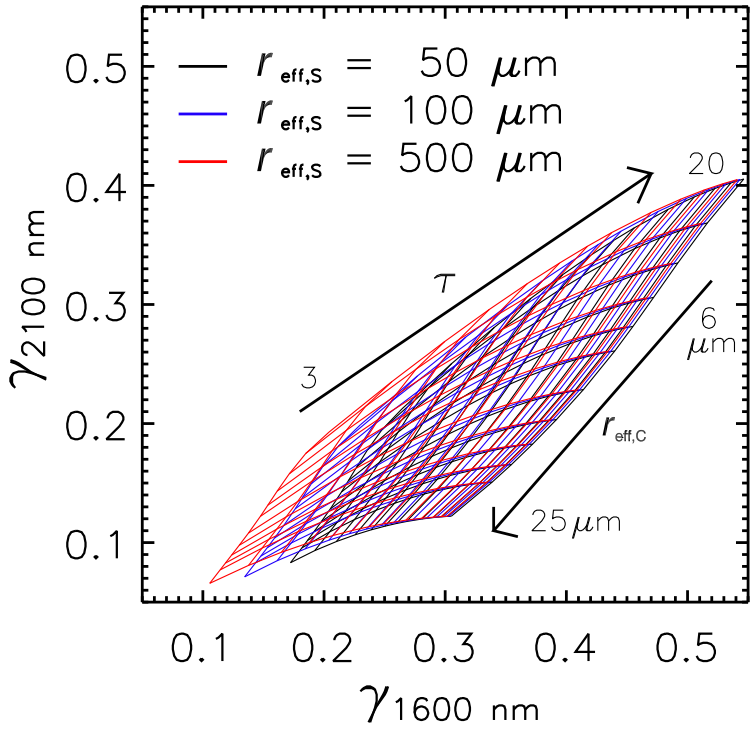

Figure 2. Bi-spectral retrieval grids of cloud top nadir reflectivity $\gamma_{1600\,\mathrm{nm}}$ and $\gamma_{2100\,\mathrm{nm}}$ assuming three different ~~snow~~ effective snow grain sizes $r_{\mathrm{eff,S}}$ of 50, 100, and 500 µm. The simulated reflectivities cover cloud optical thickness τ between 3 and 20 and cloud droplet effective radius $r_{\mathrm{eff,C}}$ between 6 µm and 25 µm.

affected by changes of $r_{\mathrm{eff,S}}$ as the snow albedo is close to zero for $r_{\mathrm{eff,S}} > 100\,\mu\mathrm{m}$ (see Figure 1). ~~This behavior suggests, that~~ As the retrieval of τ ~~, that~~ is strongly linked to $\gamma_{1600\,\mathrm{nm}}$, ~~is primarily affected by the snow albedo~~the effect of the snow albedo on the retrieved τ is obvious. However, the non-rectangular shape of the grids ~~indicate that~~ indicates, that both reflectivities are coupled to both cloud parameters and, thus, also the retrieved $r_{\mathrm{eff,C}}$ will be affected by ~~a changing snow effective grain size as the reflectivities at both wavelengths are coupled to both cloud parameters~~changes of the effective snow grain size.

2.2 Snow grain size effect on cloud retrieval results

~~To quantify the snow grain size effect on uncertainties of~~ For liquid water cloud ~~retrieval results~~ retrievals obtained over snow surfaces with unknown grain size, ~~a set of retrieval assuming different values of snow effective grain sizes were performed for~~ the snow grain size effect on uncertainties of retrieval results was quantified. Therefore, synthetic measurements obtained from the retrieval forward simulations as introduced in Section 2.1 are applied. For each synthetic measurement defined by τ, $r_{\mathrm{eff,C}}$, and $r_{\mathrm{eff,S}}$ a set of retrieval assuming different values of effective snow grain sizes were performed. The purpose of this exercise is to use the synthetic measurement (for which the original ~~snow effective grain size~~ $r_{\mathrm{eff,S}}$ is known), and ~~pretend not to know~~

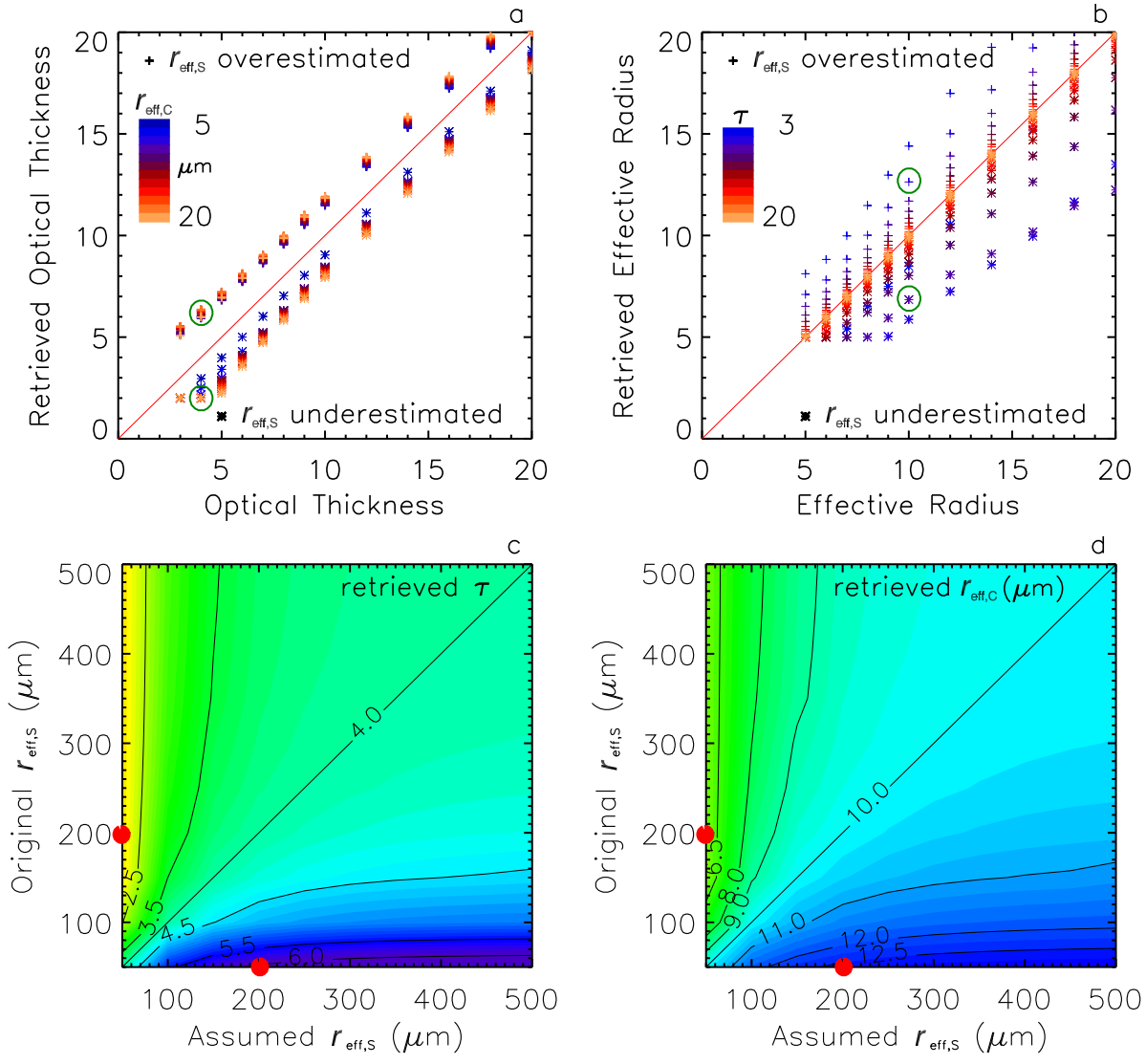

Figure 3. Comparison of synthetically retrieved τ (a, c) and $r_{\mathrm{eff,C}}$ (b, d) with the original parameter value. Calculations in panel a and b are performed for assuming a larger ~~snow~~ effective snow grain size of $r_{\mathrm{eff,S}} = 200\,\mu\mathrm{m}$ instead of the original $r_{\mathrm{eff,S}} = 50\,\mu\mathrm{m}$ (crosses) and a smaller ~~snow~~ effective snow grain size of $r_{\mathrm{eff,S}} = 50\,\mu\mathrm{m}$ instead of the original $r_{\mathrm{eff,S}} = 200\,\mu\mathrm{m}$ (asterisks). In panel c and d all combinations of assumed and original $r_{\mathrm{eff,S}}$ are analyzed for a specific cloud of $\tau = 4$ and $r_{\mathrm{eff,C}} = 10\,\mu\mathrm{m}$. The red dots in panel c and d indicate the cases included in panel a and b, where results for the same cloud are indicated by green circles.

start the retrieval assuming $r_{\mathrm{eff,S}}$ ~~when starting the retrieval . In the retrieval forward simulations different $r_{\mathrm{eff,S}}$ are assumed to quantify the impact of this wrong assumption~~ is not known. The impact of these wrong assumptions on the retrieved cloud properties ~~.~~ is then quantified.

In Figures 3a and 3b the retrieval results are compared to the original cloud properties for synthetic measurements calculated with an original ~~snow effective~~ effective snow grain size of 50 µm, but retrieved from forward simulations assuming a ~~snow effective~~ effective snow grain size of 200 µm (crosses). The asterisks symbols in Figures 3a and 3b indicate the opposite case: originally $r_{\mathrm{eff,S}} = 200\,\mu\mathrm{m}$ is used to produce the synthetic measurement and then $r_{\mathrm{eff,S}} = 50\,\mu\mathrm{m}$ is assumed in the retrieval of the cloud properties. While Figure 3a shows retrieved τ for different $r_{\mathrm{eff,C}}$ indicated by the color code, Figure 3b presents retrieved $r_{\mathrm{eff,C}}$ for clouds of different τ also indicated by a color code.

Assuming $r_{\mathrm{eff,S}}$ to be larger than originally present, the retrieved τ is systematically overestimated because the surface albedo is underestimated in this case (larger $r_{\mathrm{eff,S}}$ assumes lower snow albedo at 1600 nm, see also Figure 1). If $r_{\mathrm{eff,S}}$ is underestimated (surface albedo overestimated) the snow grain size effect is inverted leading to an underestimation of τ. This is in agreement with the general surface albedo sensitivity of cloud retrieval as discussed by Rolland and Liou (2001) and Fricke et al. (2014). For the case presented in Figure 3, ~~errors in the retrieval range~~ the snow grain size effect, expressed by the percentage deviation of the retrieved from the original true value, ranges up to 83 % for low optical thickness $\tau = 3$.

The results for τ do not significantly depend on $r_{\mathrm{eff,C}}$. ~~Contrarily~~By contrast, the uncertainties introduced in the retrieval of $r_{\mathrm{eff,C}}$ strongly depend on τ as illustrated in Figure 3b. Especially for clouds of low optical thickness, the retrieved $r_{\mathrm{eff,C}}$ is significantly overestimated/underestimated when the ~~snow effective~~ effective snow grain size is assumed to be higher/lower than originally present. The snow grain size effect ranges up to 62 % for optically thin clouds ~~with small $r_{\mathrm{eff,C}}$~~($\tau = 3$) with small $r_{\mathrm{eff,C}} = 5\,\mu\mathrm{m}$. In case ~~larger snow effective~~ of larger effective snow grain sizes are assumed, the absorption observed in $\gamma_{1600\,\mathrm{nm}}$ is overestimated while $\gamma_{2100\,\mathrm{nm}}$ is almost unchanged. This combination leads to an estimate of too low $r_{\mathrm{eff,C}}$ in the retrieval.

While the retrieval of τ ~~, independently of $r_{\mathrm{eff,C}}$,~~ is always biased due to uncertainties of $r_{\mathrm{eff,S}}$, independently of $r_{\mathrm{eff,C}}$, no snow grain size effect is observed for the retrieval of $r_{\mathrm{eff,C}}$ in case of τ ~~is~~ larger than about 10. For optically thick clouds, the high extinction of incoming radiation inside the cloud layer leads to a low amount of radiation that reaches the surface and interacts with the snow and is transmitted back ~~through top of the cloud~~ to the cloud top. In this case the interaction of radiation with the surface can be neglected and, therefore, the surface albedo, respectively the assumption of $r_{\mathrm{eff,S}}$, is not relevant.

The cases discussed in Figure 3a and 3b represent the typical range of $r_{\mathrm{eff,S}}$ from 50 µm to 200 µm as expected in Arctic areas for snow surfaces. However, white sea ice and snow cover in mid-latitudes may exhibit a higher variability leading to larger uncertainties. Therefore, Figures 3c and 3d summarize the snow grain size effect on the retrieval of τ (Figure 3c) and $r_{\mathrm{eff,C}}$ (Figure 3d) for a set of combinations of assumed and original $r_{\mathrm{eff,S}}$. A typical cloud with low optical thickness of $\tau = 4$ and $r_{\mathrm{eff,C}} = 10\,\mu\mathrm{m}$ (green circles in Figure 3a and 3b) was analyzed. The red dots indicate the cases that are included in Figure 3a and 3b~~, where results for the same cloud are indicated by green circles. An exemplary cloud with low optical thickness of $\tau = 4$ and $r_{\mathrm{eff,C}} = 10$ was analyzed.~~ .

The over- and underestimation of $r_{\mathrm{eff,S}}$ leads to almost symmetric effects for the clouds investigated here. The maximum snow grain size effect on the retrieval of τ covered by the simulations leads to a retrieval of $\tau = 2$ or $\tau = 6$ ~~. For $r_{\mathrm{eff,C}}$ the results~~ significantly deviating from the original value of $\tau = 4$. Compared to the original $r_{\mathrm{eff,C}} = 10\,\mu\mathrm{m}$ the results for $r_{\mathrm{eff,C}}$ range between 6 µm and 13 µm. The effects are most pronounced when either smaller ~~snow effective~~ effective snow grain sizes

are assumed or originally present; e.g., 50 µm assumed but 300 µm present, or 300 µm assumed and 50 µm present. Similar mismatch between assumed and original $r_{\mathrm{eff,S}}$ at larger grain sizes, e.g., 300 µm vs. 500 µm, ~~do cause much~~ cause lower errors in the retrieved τ and $r_{\mathrm{eff,C}}$. This indicates ~~,~~ that especially in polar areas where snow grain sizes are ~~typical~~ typically smaller, the retrieval biases due to a wrong assumption of $r_{\mathrm{eff,S}}$ ~~can not~~ cannot be neglected.

The numbers presented here were obtained for a solar zenith angle of $\theta_0 = 63°$. For simulations with different solar zenith angles in the range between 80° to 80° similar grain size effects are observed. In general, the magnitude of the grain size effect of τ does not significantly change with θ_0. However, for low Sun, large θ_0, the grain size effect on the retrieved $r_{\mathrm{eff,C}}$ was slightly reduced, while for higher Sun, small θ_0, the effects increase. This is caused by the increased probability that radiation interacts with the surface in case of a decreasing solar zenith angle.

3 Separating the spectral signatures of liquid water clouds and snow

In ~~case~~ cases where liquid water clouds are located above a snow surface, the spectral differences of absorption of solar radiation by snow (ice water) and clouds (liquid water) as illustrated in Figure 1 can be used to separate the surface and cloud contributions to the reflected radiation above the cloud. In addition, the different size ranges of cloud droplets (typically $r_{\mathrm{eff,C}} < 20\,\mu\mathrm{m}$) and snow grains (typically $r_{\mathrm{eff,S}} > 50\,\mu\mathrm{m}$) amplify these spectral signatures of ice and liquid water. ~~Inside large snow grains the~~ The photon path length inside large snow grains is prolonged, which leads to a stronger absorption and a lower reflectivity compared to the smaller liquid water droplets.

Using the cloud reflectivity simulations introduced in Section 2, two ~~measures~~ metrics to identify wavelengths that are most sensitive to only one single parameter, either τ, $r_{\mathrm{eff,C}}$ or $r_{\mathrm{eff,S}}$, are derived. The first parameter σ is provided by the mean standard deviation of γ_λ with respect to a single parameter τ, $r_{\mathrm{eff,C}}$, and $r_{\mathrm{eff,S}}$. E.g., for each cloud, a standard deviation of all simulations with different $r_{\mathrm{eff,S}}$ was calculated. $\sigma_{r_{\mathrm{eff,S}}}$ is then derived by averaging these standard deviations for all different clouds. The second parameter are the spectral weightings of a principle component analysis (PCA) applied to the full set of simulations. Corresponding to the cloud and snow parameters changed in the simulations, the spectral weights Γ_1, Γ_2, and Γ_3 of the first three principle components are found to be associated with τ (Γ_1), $r_{\mathrm{eff,C}}$ (Γ_2), and $r_{\mathrm{eff,S}}$ (Γ_3).

Both ~~measures~~ metrics are shown in Figure 4 for τ (σ_τ and Γ_1), for $r_{\mathrm{eff,C}}$ ($\sigma_{r_{\mathrm{eff,C}}}$ and Γ_2), and for $r_{\mathrm{eff,S}}$ ($\sigma_{r_{\mathrm{eff,S}}}$ and Γ_3). The results are presented for a solar zenith angle of $\theta_0 = 63°$ but are applicable to larger and smaller θ_0. The three calculated functions of σ show that the maximum variability of the cloud reflectivity with respect to the three parameters is located in different spectral regions. While $r_{\mathrm{eff,S}}$ mostly affects the cloud reflectivity at wavelengths between 930 nm and 1350 nm, τ introduces high standard deviations in the wavelength range of $1500 - 1800\,\mathrm{nm}$. However, this spectral range is also influenced by $r_{\mathrm{eff,C}}$ with $\sigma_{r_{\mathrm{eff,C}}}$ showing values only moderately lower ~~values~~ than σ_τ. Values of similar magnitude are observed for $\sigma_{r_{\mathrm{eff,C}}}$ at ~~longer wavelength larger~~ wavelength larger then 2000 nm. In this spectral range $r_{\mathrm{eff,C}}$ is the dominating parameter determining the cloud reflectivity.

Similar spectral ~~pattern~~ patterns result from the PCA, which delivers the spectral ~~weighs~~ weights Γ_1, Γ_2, and Γ_3 ~~as~~ , are presented in Figure 4b. A comparison with the three calculated σ in Figure 4b reveals that Γ_1 can be associated with τ, Γ_3

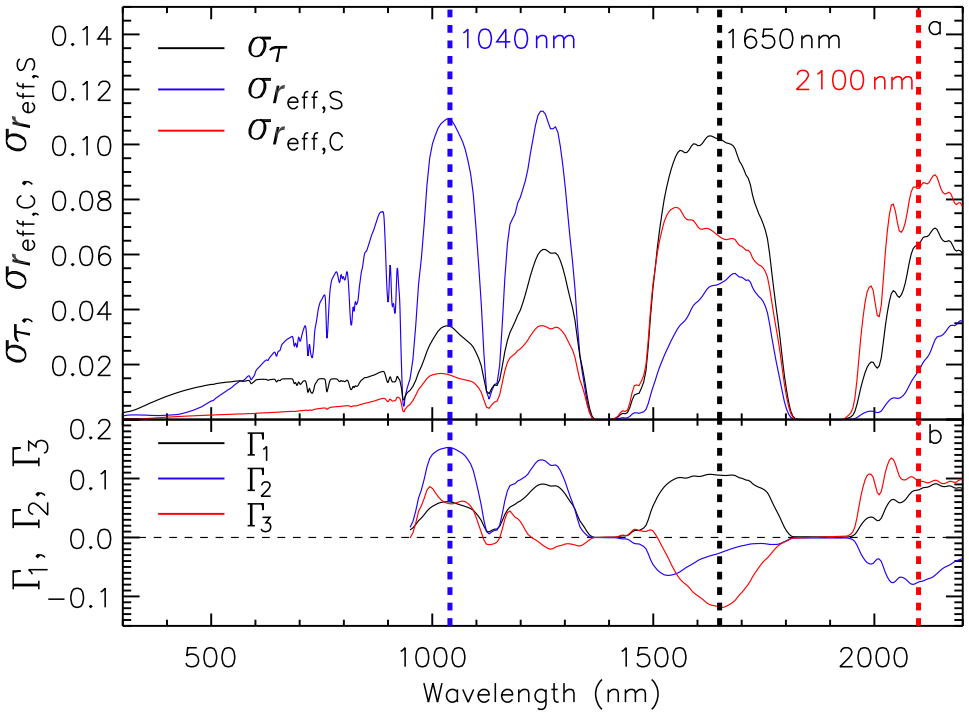

Figure 4. Mean standard deviations of spectral cloud reflectivity σ_τ, $\sigma_{r_{\mathrm{eff,C}}}$, and $\sigma_{r_{\mathrm{eff,S}}}$ with respect to a single cloud or snow parameter τ, $r_{\mathrm{eff,C}}$, and $r_{\mathrm{eff,S}}$ calculated for the sets of radiative transfer simulations (panel a). First three spectral weights Γ_1, Γ_2, and Γ_3 of a principle component analysis are given in panel b.

with $r_{\mathrm{eff,C}}$ and Γ_2 with $r_{\mathrm{eff,S}}$. The major contribution to Γ_1 is located in the wavelength range $930-1350\,\mathrm{nm}$ dominated by the changes in snow albedo, $r_{\mathrm{eff,S}}$. The impact of τ is spectrally neutral, showing a similar magnitude of Γ_1 in all analyzed wavelengths expect of the water vapor absorption bands. ~~Contrarily~~By contrast, wavelengths above $1500\,\mathrm{nm}$ contribute most to the weight of the third principle component Γ_3, but with opposite signs for the $1500-1800\,\mathrm{nm}$ and the $2000-2200\,\mathrm{nm}$ wavelength range.

It has to be mentioned ~~,~~that these sensitivities might change for different scenarios assumed in the radiative transfer simulations, e.g., different solar zenith angle, cloud altitude, profile of cloud droplet size, or aerosol concentration. Similarly, the use of sub samples of the full cloud and snow parameter range investigated here might change the derived values. However, the general separation of the three parameters by different spectral ranges will not essentially differ.

4 Tri-spectral retrieval algorithm

4.1 Selected wavelengths and radiance-ratios

Based on the spectral ~~signatures imprinted in the cloud reflectivity by variations~~ footprint of τ, $r_{\mathrm{eff,C}}$ and $r_{\mathrm{eff,S}}$ in the cloud reflectivity, a tri-spectral retrieval algorithm ~~using measured γ_λ~~ is proposed to ~~retrieve~~ derive the three cloud and snow parameter simultaneously. ~~Extending~~ In this way, the conventional bi-spectral cloud ~~retrievals~~ retrieval was extended by a third measurement at a wavelength sensitive to $r_{\mathrm{eff,S}}$, which adds the information on the snow grain size. Compared to retrieval algorithms that rely on a fixed assumption of $r_{\mathrm{eff,S}}$~~this approach can reduce~~, this new tri-spectral approach reduces the uncertainty of the retrieved cloud parameters.

~~Measurements~~ In particular, measurements at $\lambda_1 = 1040\,\mathrm{nm}$ which are most sensitive to $r_{\mathrm{eff,S}}$, $\lambda_2 = 1650\,\mathrm{nm}$ most sensitive to τ, and $\lambda_3 = 2100\,\mathrm{nm}$ most sensitive to $r_{\mathrm{eff,C}}$ were chosen in the retrieval algorithm. ~~To improve the separation of the individual cloud and snow parameters~~

In the new tri-spectral retrieval algorithm, the radiance-ratio method introduced by ~~Werner et al. (2013); Brückner et al. (2014); LeBlanc et~~ Werner et al. (2013), Brückner et al. (2014), and LeBlanc et al. (2015) was applied. ~~Here a~~ A normalization with the cloud reflectivity at $\lambda_0 = 860\,\mathrm{nm}$ was chosen. The corresponding ratios R_1, R_2, and R_3 are calculated ~~by,~~ as

$$R_1 = \frac{\gamma_{\lambda_1}}{\gamma_{\lambda_0}}, \qquad R_2 = \frac{\gamma_{\lambda_2}}{\gamma_{\lambda_1}}, \qquad R_3 = \frac{\gamma_{\lambda_3}}{\gamma_{\lambda_2}}, \tag{2}$$

with $\lambda_0 = 860\,\mathrm{nm}$, $\lambda_1 = 1040\,\mathrm{nm}$, $\lambda_2 = 1650\,\mathrm{nm}$, and $\lambda_3 = 2100\,\mathrm{nm}$.

~~These~~ The normalizations additionally reduce the uncertainties of the retrieval by cancelling potential biases in the radiometric calibration of the measurements. ~~Alternatively, e. g., when restricted to MODIS channels, for λ_2 related to $r_{\mathrm{eff,S}}$ a wavelengths between 1200~~Except for λ_1, all wavelengths that were chosen for the algorithm are covered by the satellite imagers MODIS and VIIRS. To apply the algorithm to global observations by these instruments, λ_1 can be exchanged by the 1240 nm ~~and 1300 can be chosen~~ wavelength band where cloud reflectivity is still most sensitive to $r_{\mathrm{eff,S}}$.

Similar to Section 3, the mean standard deviation σ with respect to ~~a single parameter~~ τ, $r_{\mathrm{eff,C}}$, and $r_{\mathrm{eff,S}}$ was calculated for the three reflectivity ratios. Table 1 shows σ for all possible parameter combinations. The higher σ, the more sensitive R_1, R_2, and R_3 are ~~for~~ with respect to changes of an individual cloud or snow parameter. ~~For~~ One ratio with significantly higher σ is found for each parameter, τ, $r_{\mathrm{eff,C}}$, and $r_{\mathrm{eff,S}}$~~, one reflectivity ratios shows a significant higher σ compared to the other ratios~~. For the cloud optical thickness ~~,~~ the highest $\sigma = 0.145$ is found for R_2~~and~~, which is almost twice as high ~~compared to~~ as the sensitivity of R_1 and R_3. Similarly, R_1 ~~and R_3 show~~ shows the highest sensitivity to $r_{\mathrm{eff,S}}$ and R_3 the highest σ for $r_{\mathrm{eff,S}}$ and $r_{\mathrm{eff,C}}$ ~~, respectively,~~ with $\sigma = 0.074$ and $\sigma = 0.121$, respectively. This indicates ~~,~~ that R_1, R_2, and R_3 are well suited to separate the information of τ, $r_{\mathrm{eff,C}}$, and $r_{\mathrm{eff,S}}$ from spectral reflectivity measurements.

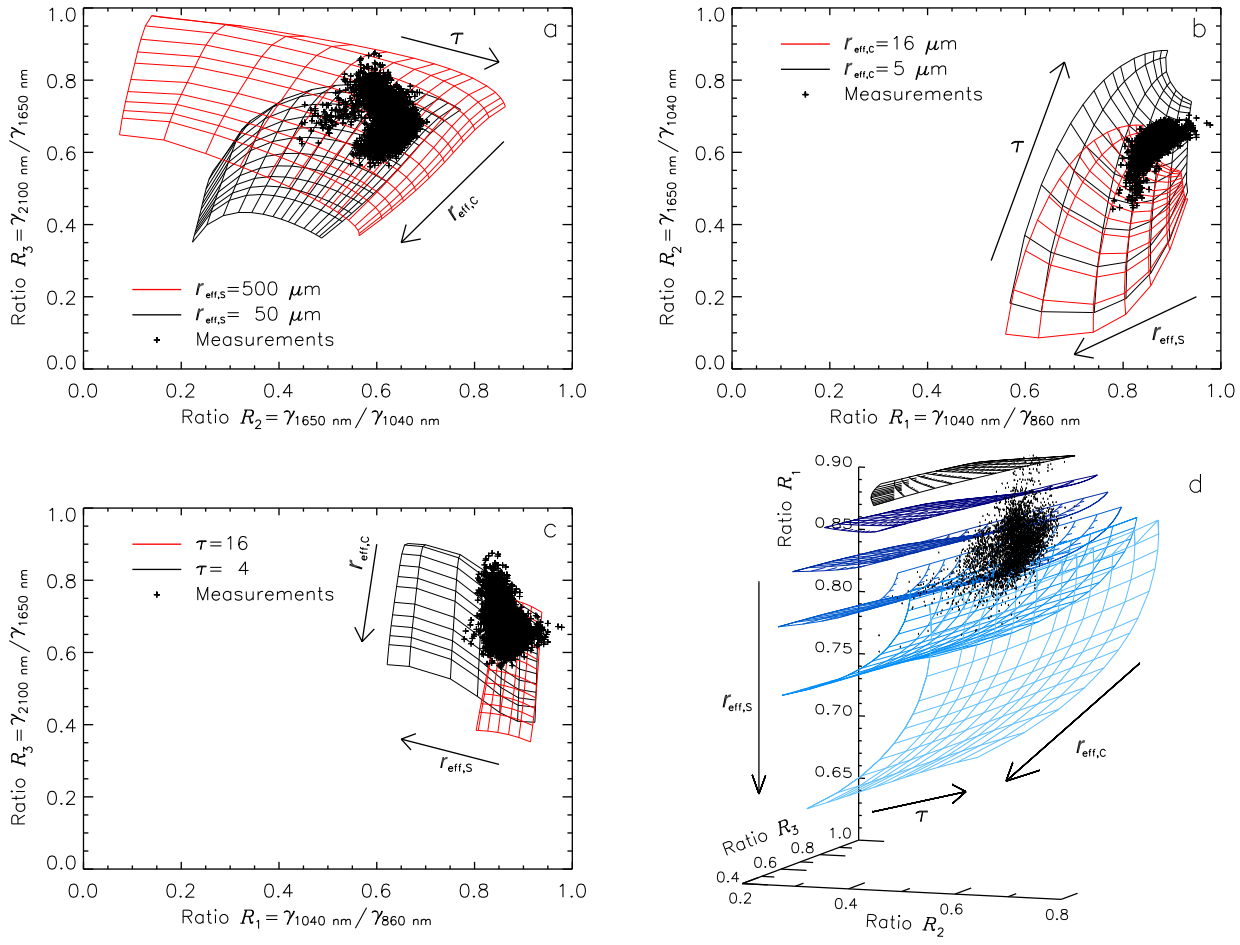

Figure 5. Three-dimensional retrieval grid using the ratios R_1, R_2, and R_3 obtained from simulations covering $\tau = 1$-~~20~~-20, $r_{\mathrm{eff,C}} =$ 5-~~25~~-25 µm and $r_{\mathrm{eff,S}} = 25$-~~800~~-800 µm. Panel ~~a-c~~ a-c show each two selected two-dimensional section of the retrieval grid, while panel d covers the full 3D grid. ~~Exemplary~~ Representative measurements obtained during VERDI (29 April 2012) are ~~imprinted~~ represented by black dots.

4.2 Retrieval grid

The set of cloud reflectivity simulations introduced in Section 2 served for the forward simulations (solar zenith angle of 63°, liquid water cloud layer between 200 m and 500 m). The simulated grids of R_1, R_2, and R_3 used for the tri-spectral retrieval are presented in Fig 5. While Fig. 5d shows the full 3-dimensional (3D) grid covering $\tau =$ 1-20, $r_{\mathrm{eff,C}} =$ 5-25 µm and $r_{\mathrm{eff,S}} =$ 25-800 µm, Fig. 5a-c present ~~2-dimensional projections of two~~ two-dimensional projections of reflectivity ratios with one parameter being fixed. In Fig. 5a, $r_{\mathrm{eff,S}}$ is ~~fixed~~ set to 50 µm (black) and 500 µm (red), while in Fig. 5b $r_{\mathrm{eff,C}}$ is fixed ~~to~~ at 5 µm (black), and 16 µm (red) and in Fig. 5c τ is fixed to ~~a value~~ values of 4 (black) and 16 (red). ~~In all figures the~~

Table 1. Standard deviation of the reflectivity ratios R_1, R_2, and R_3 with respect to one of the three cloud and snow parameter τ, $r_{\mathrm{eff,C}}$, and $r_{\mathrm{eff,S}}$.

	$r_{\mathrm{eff,S}}$	τ	$r_{\mathrm{eff,C}}$
R_1	**0.074**	0.039	0.015
R_2	0.065	**0.145**	0.088
R_3	0.054	0.056	**0.121**

~~directions of change by τ, $r_{\mathrm{eff,C}}$, and $r_{\mathrm{eff,S}}$ are indicated by arrows. The simulated grid shows~~ The simulated grids show that the individual lines ~~cross almost perpendicular for large~~ almost align orthogonally for wide ranges of the simulated ~~parameters. No overlapping of the different surfaces is observed~~parameter space. The different surfaces do not overlap. This indicates that the three chosen ratios R_1, R_2, and R_3 separate the influence of the three parameters τ, $r_{\mathrm{eff,C}}$, and $r_{\mathrm{eff,S}}$ on the cloud reflectivity and allow a retrieval of the cloud and snow parameters leaving ~~little~~ few ambiguities. Only for ~~small snow effective grain sizes~~ $r_{\mathrm{eff,S}}$ lower than 50 µm the grid ~~becomes~~ is more narrow as obvious in Fig. 5d (uppermost black grid) and Fig. 5a (black grid). Such a narrow grid increases the uncertainty of the retrieved τ and $r_{\mathrm{eff,C}}$ especially for clouds of low optical thickness. This grid characteristic is caused by the higher surface albedo of snow for small values of $r_{\mathrm{eff,S}}$, which reduces the contrast between cloud and snow surface ~~also in the wavelength range used~~ for the ~~retrieval algorithm~~wavelengths used to calculate the three ratios. However, a retrieval of cloud and snow properties ~~in these ranges~~ is still possible in these ranges if the measurement uncertainties are sufficiently ~~low.~~ small. A more general quantification of the retrieval sensitivities and uncertainties can be derived by optimal estimation techniques, which is, however, beyond of the scope this paper.

Ambiguities appear in the retrieval for small cloud droplet effective radii of $r_{\mathrm{eff,C}} < 5\,\mu\mathrm{m}$ (not shown in Fig. 5). In that case the absorption of cloud droplets is ~~to week and cloud reflectivity can be~~ weak and the cloud reflectivity is similar to a cloud with larger $r_{\mathrm{eff,C}}$ but smaller τ. Therefore, ~~when applying the retrieval~~ all solutions with with $r_{\mathrm{eff,C}} < 5\,\mu\mathrm{m}$ were excluded from the retrieval.

4.3 Adjustments and uncertainty estimation

The retrieval algorithm was additionally adjusted to Arctic conditions where open water and ice ~~flows may be present~~ floes can occur in close proximity. ~~Therefore, the algorithms first distinguishes if~~ First, the algorithm determines whether the measurements are obtained over snow-covered sea ice or open water surfaces. Even in ~~case of overlying clouds, a separation of~~ the case of cloud covered scenes, the border between sea ice and open water is clearly discernable in the cloud top reflectivity as shown by Schäfer et al. (2015). A surface with a high albedo always enhances the upward radiance above a cloud ~~also for optical~~ even in the case of optically thick clouds. Therefore, a fixed threshold of cloud reflectivity $\gamma(\lambda_0) \geq 0.65$ at a wavelength ~~below roughly 1000~~of 860 nm ~~can be~~ is applied to distinguish ~~measured cloud reflectivities~~ measurements obtained above snow or white sea ice ~~and~~ from those over open water. ~~Based on the simulations presented above, the spectral reflectivity~~

at 860 wavelength and a threshold of $\gamma(\lambda_0) > 0.65$ was chosen to classify measurements above snow and open water. This value might change if This value may need to be adjusted for conditions of different solar zenith angles are different to the simulations presented here and if or clouds with higher optical thicknessare considered.

If $\gamma(\lambda_0)$ the cloud reflectivity at 860 nm is below the threshold, an open water surface is assumed. In that case a the bi-spectral retrieval following the radiance ratio approach of Werner et al. (2013) was is applied. Cloud reflectivities $\gamma(\lambda_2)$ and the reflectivity ratio $R_3 = \gamma(\lambda_3)/\gamma(\lambda_2)$ were are used to retrieve τ and $r_{\text{eff,C}}$. If $\gamma(\lambda_0)$ is above the threshold, a snow surface is assumed. In that case Then the measurements are converted into the three reflectivity ratios R_1, R_2, and R_3 and interpolated to the 3D grid of simulated values introduced in Sec. 4.2.

However, as quantified by Schäfer et al. (2015), in the vicinity of 3D radiative effects in vicinity to sea ice edges 3D radiative effects do significantly influence the reflected radiation . This effect may range up to horizontal distances of a couple of km depending and bias the retrieved cloud properties (Schäfer et al., 2015). Depending on cloud and surface geometry, this effect is important up to several kilometers distance from the ice edge. Therefore, such measurement sections measurements collected close to sea ice edges have been removed from the analysisas retrieved cloud properties might be biased by up to 90 in the close vicinity of sea ice edge.

Retrieval The retrieval uncertainties are estimated by considering the uncertainties of each measured reflectivity ratio expressed by its considering the measurement errors of the reflectivity ratio and assuming a Gaussian distribution of the errors. In this case the uncertainties can be expressed by their double standard deviation 2σ. The retrieval is operated for varying each ratio, R_1, R_2, and R_3, separately by adding and subtracting 2σ. This procedure ends up results in six solutions for the tri-spectral retrieval over snow surfaces and four solutions for the bi-spectral retrieval over open water. This set of solutions is sufficient to represent the full solution space of the Gaussian distributed measurement uncertainties. The median of these solutions was used as is used as the retrieval result of τ, $r_{\text{eff,C}}$, and $r_{\text{eff,S}}$, while the standard deviation of all solutions quantifies the retrieval uncertainty $\Delta\tau$, $\Delta r_{\text{eff,C}}$, and $\Delta r_{\text{eff,S}}$.

Independent of these uncertainties caused by the measurementsitself, systematic uncertainties , systematic errors due to the assumptions in the forward simulations have to be considered. Firstare considered. Currently, the retrieval algorithm is limited to liquid water clouds only and, therefore, may suffer from an incorrect assumption of the cloud phaseif the cloud contains ice. In the Arctic, mixed-phase clouds that are dominated by a liquid water layer at cloud top are frequent (Mioche et al., 2015). In that this case, the retrieval algorithm may fail may provide unrealistic cloud properties as the ice crystals in these clouds absorb solar radiation at similar wavelengths as the snow surface does. The absorption by the ice crystals may add to the absorption of by the snow surface and bias the retrieval results.

SecondFurthermore, limitations of the snow albedo parametrization by Zege et al. (2011) applied in the forward simulations may introduce biases in the retrieved $r_{\text{eff,S}}$. E.g., the The parametrization assumes a fixed snow grain shape quantified by the form-factor $A = 5.8$. Typical values of A range approximately between from 5.1 for fractals to 6.5 for spheres. For a cloud free retrieval of snow grain size , which represents the maximum effect expected for cloudy conditions, this in cloud free conditions, the snow grain shape implies uncertainties in the retrieved snow effective effective snow grain size up to 25 %. However, as discussed by Zege et al. (2011), although the uncertainty of the snow grain shape may produce uncertainties in the retrieved

$r_{\mathrm{eff,S}}$, the the reflection characteristics of the snow, in particular the spectral albedo, are not affected at wavelengths used by the retrieval algorithm. Both properties , A and $r_{\mathrm{eff,S}}$ change the snow albedo with similar spectral pattern. This similarity patterns, which allows to attribute the uncertainty of A as uncertainties uncertainty of $r_{\mathrm{eff,S}}$. Therefore, the retrieved cloud properties are independent of the assumption of A. This emphasises,

This emphasises that the retrieved $r_{\mathrm{eff,S}}$ has always always has to be considered as an effective quantity. It represents the snow grain size that has to be used in the specific albedo parametrisation (fixed form-factor A) to provide the snow albedo which is most representative for the measurements. Spatial or temporal differences in of the retrieved $r_{\mathrm{eff,S}}$ may result either by from a change of the geometric size of the snow grains or by from changes of the snow grain shape quantified by the form-factor.

5 Application to airborne measurementsduring VERDI

Airborne spectral solar radiation measurements were collected with the Spectral Modular Airborne Radiation measurement sysTem (SMART-AlbedometerSMART) during the airborne research campaign Vertical Distribution of Ice in Arctic Clouds (VERDI). In April/May 2012 in total A total of 16 research flights was conducted in April/May 2012 with the Polar 5 aircraft operated by Alfred-Wegener Institute for Marine and Polar Research (AWI) were performed over the Canadian Beaufort Sea, which was partly covered with snow-covered sea iceand partly ice free.

The SMART-Albedometer measured SMART measured the spectral solar radiance reflected in nadir direction (2.1° field of view) and downward spectral irradiance with grating spectrometers covering the wavelength range between 350 nm and 2200 nm (Ehrlich et al., 2008; Wendisch et al., 2001)(Wendisch et al., 2001; Ehrlich et al., 2008). From both quantities cloud reflectivity γ was calculated using Eq. 1. The SMART-Albedometer SMART was calibrated radiometrically, spectrally and geometrically in laboratory. the laboratory.

The uncertainties of the measurements mostly originate from the radiometric calibration given by the uncertainty of the applied radiation source (traceable to the standards of the National Institute of Standards and Technology, NIST) and the signal to noise ratio that differs with wavelength due to the sensitivity of the spectrometers.

By calculating the ratios R_1, R_2, and R_3, as used in the retrieval algorithm, calibration uncertainties partly cancel. E.g., a bias in the radiometric calibration will affect cloud reflectivities at different wavelengths to the same degree, but does not change influence the ratios. Summing up all effects and considering typical measurements Altogether, assuming typical measurements of clouds above snow, a 2σ uncertainty of 6 % was estimated for R_1, while for R_2 and R_3, 4 % and 12 % uncertainty uncertainties were considered. For the retrieval of clouds over open water, where $\gamma(\lambda_2)$ and the reflectivity ratio R_3 are used, the darker surface (lower signal and lower signal to noise ratio) lead to uncertainties in the observations of 9 % for $\gamma(\lambda_2)$ and 13 % for R_3.

Two different 30 min extracts from the sections from observations on 29 April (Case I) and 17 May 2012 (Case II) were selected to test the retrieval algorithm. In both cases a wide area close to the coast line was covered by stratiform boundary layer clouds. While for Case I the cloud top, defined by the boundary layer inversion, reached altitudes of up to 700 m,

persistent subsidence driven by anticyclonic conditions lead to a low cloud top of 200 m in Case II. During the remote sensing observations of these clouds, the Polar 5 aircraft flew ~~in~~ at an altitude of about ~~10~~3,000 ~~ft~~m. The flight tracks and the sections of the flight selected for ~~detailed analysis of the retrieval algorithms~~ a detailed analysis are included in Figures 8 and 10.

For the application of the retrieval to ~~real~~ measurements it has to be considered ~~,~~ that a pure snow surface is assumed in the forward simulations. Although a snow thickness of 2 cm will be sufficient to neglect the variation of snow albedo with snow thickness (Warren, 2013), this ~~constrain~~ constraint might not be valid ~~when~~ for observations over sea ice with leads or melt ponds~~are analyzed~~. The research flights of VERDI have been performed almost exclusively over the partly sea-ice-covered Beaufort Sea. For the two cases~~analyzed in detail~~, observations have been selected where the surface conditions are close to the required pure snow surface. However, potential effects by leads, melt ponds, or snow free sea ice are discussed for the individual cases.

Cloud microphysical in situ measurements on board of Polar 5 were use to validate the retrieved $r_{\mathrm{eff,C}}$d. A Cloud Droplet Probe (CDP) provided size resolved cloud particle concentrations in the size range from 2.5 µm to 46 µm and corresponding $r_{\mathrm{eff,C}}$ (Klingebiel et al., 2015). Using only one aircraft, the in situ and remote sensing measurements had been performed subsequently. For both investigated Cases I and II, the remote sensing flight legs were flown first. Roughly one hour later the in situ measurements were obtained at the same location following the flight track of the remote sensing sequence. Due to the stable meteorological conditions, changes of the cloud properties with time are expected to be small which allows a comparison of in situ and remote sensing data. A reference to validate the retrieved snow grain size is not available because no ground-based measurements on the sea ice have been conducted during VERDI.

5.1 Case I ~~–~~ – 29 April 2012

~~On 29 April 2012 the observations~~ The observations in this case were collected exclusively over snow-covered sea ice ~~. The selected measurements were~~ and obtained between 16:~~54-17~~54–17:21 UTC with a solar zenith angle ~~close to~~ of 63° ~~as assumed in the forward simulations of the retrieval algorithms presented in Section 4.2.~~

. The retrieved cloud and snow properties are presented in Fig. 6. Cloud optical thickness ranged between $\tau = 6$ at the ~~beginning of the presented time series~~ begin and $\tau = 15$ ~~in the second part~~at the end of the flight leg. $r_{\mathrm{eff,C}}$ also shows a tendency of increasing values ~~but changed only slightly in time~~ between 6 µm and 9 µm, while $r_{\mathrm{eff,S}}$ remained almost constant at values around 100 µm. In situ cloud microphysical measurements of $r_{\mathrm{eff,C}}$ had been obtained along the same flight track about one hour after the remote sensing measurements. At cloud top, two derived vertical profiles show $r_{\mathrm{eff,C}}$ between 6 µm and 7.5 µm, which is in the range of the retrieval results.

The retrieval uncertainties are indicated by the shaded areas in Fig. 6. In the first part of the time series, up to 17:07 UTC, the retrieval uncertainties are lowest for τ with about $\Delta\tau \pm 1$, and range at $\Delta r_{\mathrm{eff,C}} \pm 1.5\,\mu\mathrm{m}$ for $r_{\mathrm{eff,C}}$, and $\Delta r_{\mathrm{eff,S}} \pm 60\,\mu\mathrm{m}$ for $r_{\mathrm{eff,S}}$. In the second part of the time series, the retrieval uncertainty $\Delta\tau$ significantly ~~increase~~increases. This correlates with the increase of the cloud optical thickness. Similarly, $\Delta r_{\mathrm{eff,S}}$ shows a slight negative correlation with ~~higher uncertainties~~ uncertainties being higher for low τ. This is also reflected by the retrieval grids presented in Fig. 5. ~~With increasing~~ The grid spacing is more narrow for larger τ~~the grid spacing becomes more narrow~~ .

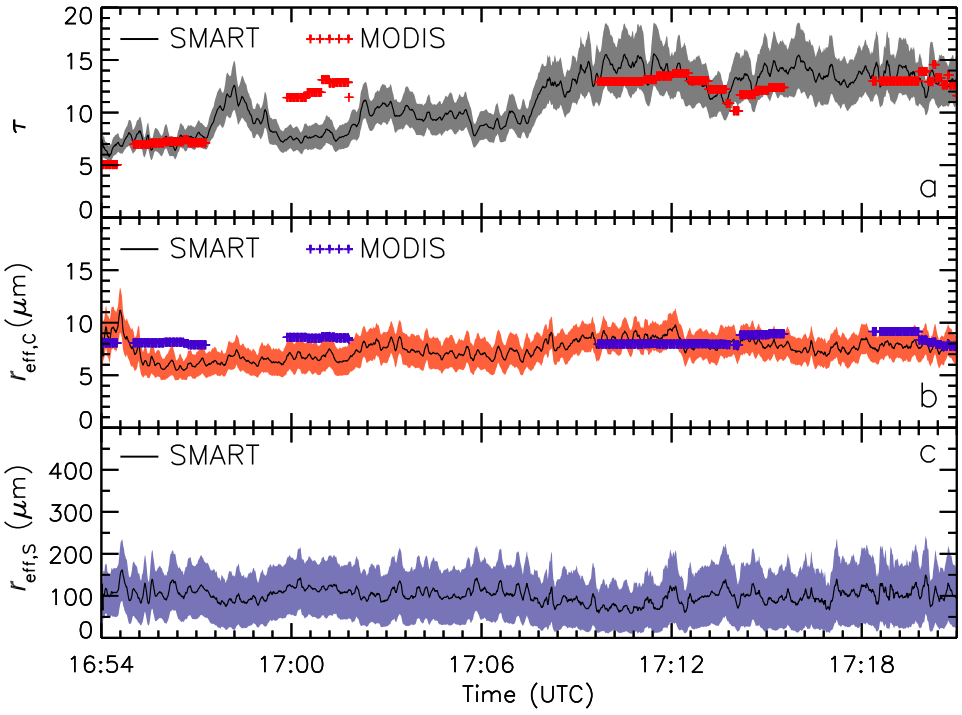

Figure 6. Time series of cloud optical thickness τ (a), cloud droplet effective radius $r_{\mathrm{eff,C}}$ (b) and ~~snow~~ effective snow grain size $r_{\mathrm{eff,S}}$ (c) retrieved ~~by~~ from SMART measurements for Case I on 29 April 2012. Uncertainties of the retrieved properties are indicated by dark shaded areas. When available, results of the MODIS cloud product are given for τ and $r_{\mathrm{eff,C}}$ (5x5 pixel average).

For all measurements, the ~~dependencies~~ behaviour of $\Delta\tau$ and $\Delta r_{\mathrm{eff,S}}$ as ~~a function~~ functions of the retrieved τ and $r_{\mathrm{eff,S}}$ ~~are~~ is shown in Figure 7. For $\Delta\tau$, values of $r_{\mathrm{eff,S}}$ are color-coded in each data point, while for $\Delta r_{\mathrm{eff,S}}$ colors indicate ~~$r_{\mathrm{eff,S}}\tau$~~. Positive correlations are found for both parameters; the larger the retrieved τ or $r_{\mathrm{eff,S}}$, the larger their uncertainties. For $\Delta\tau$ uncertainties are larger for small $r_{\mathrm{eff,S}}$ (color code in Figure 7a). In this case, small $r_{\mathrm{eff,S}}$ increase the snow albedo and lower the contrast ~~of clouds also at large wavelengths such as~~ between clouds and snow surface at $\lambda = 1650\,\mathrm{nm}$ ~~used for the retrieval of~~, which then becomes less sensitive to τ. Similarly, $\Delta r_{\mathrm{eff,S}}$ depends on the retrieved τ (color code in Figure 7b)~~:~~, with higher uncertainties observed for large τ. For high optical thickness the clouds begin to mask the surface and information of the surface is lost in the reflected radiation measured above cloud top ~~. Therefore, measurement uncertainties result in~~ leading to higher uncertainties of $r_{\mathrm{eff,S}}$. For $\Delta r_{\mathrm{eff,C}}$, similar dependencies are obtained but with less ~~variability between $\pm 1.2 - 1.7$~~spread; $\Delta r_{\mathrm{eff,C}}$ ranges between $\pm 1.2\,\mu\mathrm{m}$ and $\pm 1.7\,\mu\mathrm{m}$ (not shown here). $\Delta r_{\mathrm{eff,C}}$ was found to ~~slightly increase~~ increase slightly with decreasing $r_{\mathrm{eff,S}}$ and increasing $r_{\mathrm{eff,C}}$.

The snow-covered sea ice below the clouds ~~might~~ did have some open or only recently frozen leads, which were identified when Polar 5 did ~~fly~~ flew below clouds after the remote sensing flight leg. From automatic photographs taken on board of

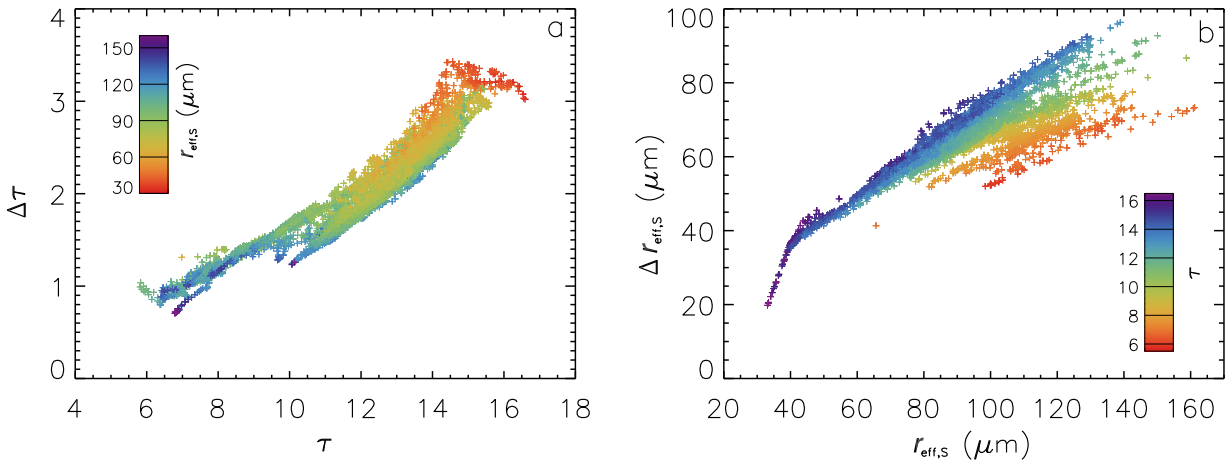

Figure 7. Uncertainties $\Delta\tau$ (a) and $\Delta r_{\mathrm{eff,S}}$ (b) as a function of retrieved τ and $r_{\mathrm{eff,S}}$. The single measurements are color-coded with $r_{\mathrm{eff,S}}$ for (a) and τ for (b).

Polar 5, the amount of leads was estimated to be lower than 5 %, which might explain some of the higher values observed in the retrieved time series of $r_{\mathrm{eff,S}}$.

The retrieved cloud and snow properties were compared to satellite observations by MODIS (Wiebe et al., 2013). Figure 8 shows maps of cloud optical thickness τ (a), droplet effective radius $r_{\mathrm{eff,C}}$ (b) and ~~snow effective~~ effective snow grain size $r_{\mathrm{eff,S}}$ (c) retrieved by MODIS. The flight track of Polar 5 is indicated by a black line and overlayed by the retrieval results of SMART. τ and $r_{\mathrm{eff,C}}$ retrieved by MODIS along the flight track are additionally included in Figure 6. Cloud properties are obtained by the MODIS cloud product Collection 6 for observations over snow or sea ice using band 6 at 1640 nm and band 7 at 2130 nm (Platnick et al., 2017). The ~~snow effective~~ effective snow grain size is provided by the Snow Grain Size and Pollution amount (SGSP) retrieval algorithm by Zege et al. (2011). The SGSP is limited to cloud free ~~pixel~~ pixels and, therefore, does not show values below the clouds observed in the same image. For Case I, the ~~AQUA~~ Aqua overpass of 20:00 UTC was analyzed. Although ~~, the MODIS data was measured~~ the MODIS scene was taken about three hours after the airborne measurements, the stable cloud conditions allow a comparison. Snow grain sizes typically change over longer time scales~~and, therefore, are directly comparable if no~~ , except precipitation occurs. The weather station in Tuktoyaktuk close to the coast line did report light precipitation of snow grains but ~~might not be~~ is not necessarily representative for the clouds over the Beaufort Sea. However, a direct comparison of $r_{\mathrm{eff,S}}$ is not possible anyway due to the missing data in cloudy ~~pixel~~pixels.

The MODIS cloud product in Figure 8 shows τ and $r_{\mathrm{eff,C}}$ in the same range as retrieved ~~by~~ from the airborne measurements. Note that here a longer time series ~~of airborne data is shown as~~ is shown than presented in Figure 6. ~~At the~~ This includes areas with snow covered land surfaces, for which the retrieval can be applied assuming that the snow layer is sufficiently thick and the snow albedo is not affected by the underlying surface (Warren, 2013). At the southern edges of the cloud field lower values of τ are observed by both MODIS and SMART. For $r_{\mathrm{eff,C}}$ the values retrieved by SMART show the same tendency of lower $r_{\mathrm{eff,C}}$ at the southern cloud edge and increasing $r_{\mathrm{eff,C}}$ towards the western end of the flight track. For large areas of this cloud

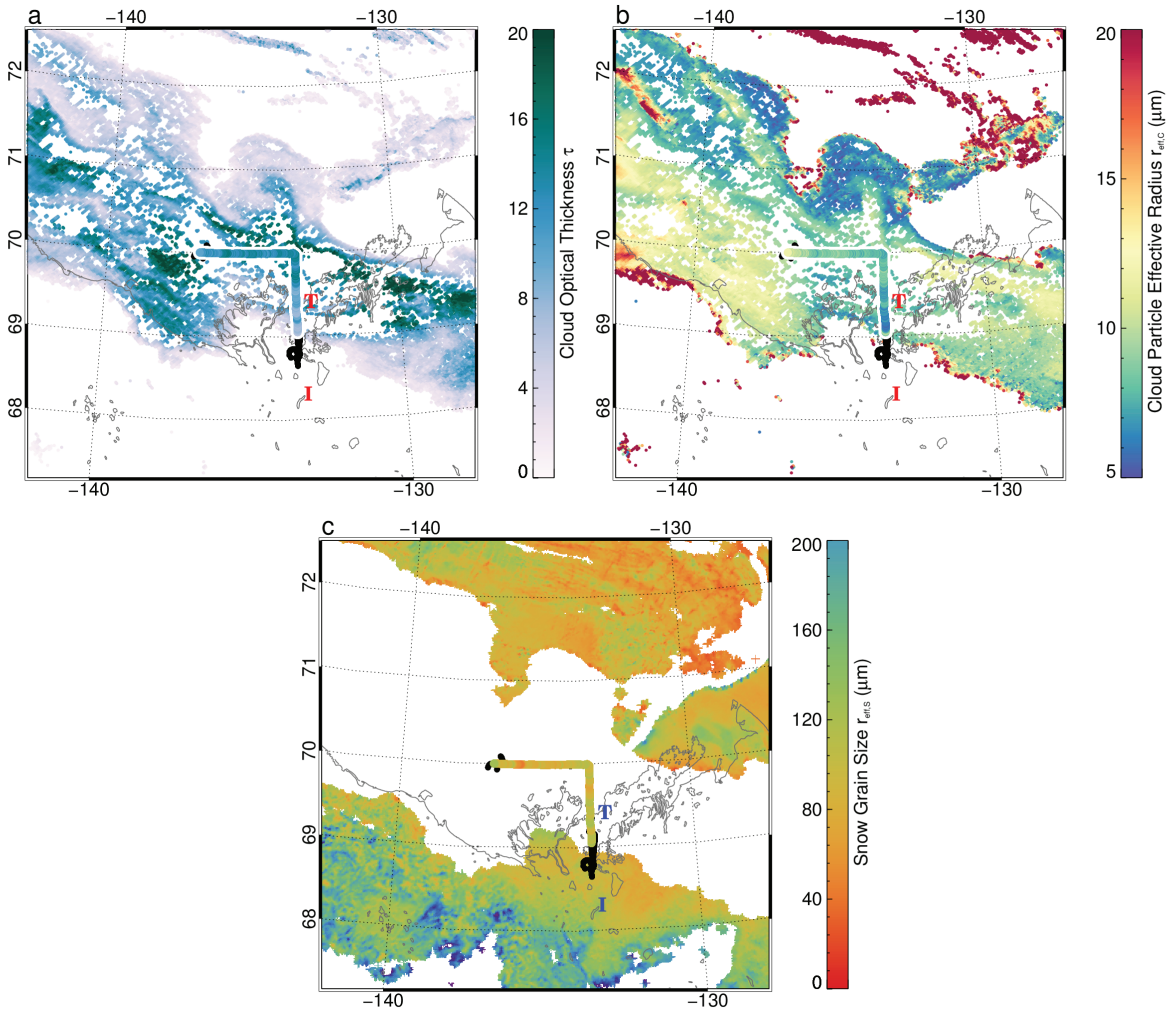

Figure 8. Cloud optical thickness τ (a), cloud droplet effective radius $r_{\mathrm{eff,C}}$ (b) and ~~snow~~ effective snow grain size $r_{\mathrm{eff,S}}$ (c) retrieved by MODIS and SMART for Case I on 29 April 2012. The total flight track is indicated by a black line and overlayed by the retrieval results of SMART. 'I' and 'T' mark the location of Inuvik and Tuktoyaktuk.

field the MODIS cloud product did not provide valid solutions~~what illustrated~~, which illustrates the limits of the current cloud retrieval in Arctic regions.

For $r_{\mathrm{eff,S}}$ no direct comparison is possible. However,the ~~SMART retrieval~~ retrieval using measurements by SMART fills the gap of the cloudy areas not considered in the SGSP retrieval for MODIS. The retrieved $r_{\mathrm{eff,S}}$ are in the same range as those observed by MODIS south and north of the cloud field and~~therefore considered to by~~, therefore, are considered to be consistent with the SGSP product. Lower $r_{\mathrm{eff,S}}$ were detected by MODIS at higher latitudes with some bias due to large leads in the sea

ice that are imprinted in the retrieval results. At lower latitudes, the snow is strongly influenced by accelerated metamorphism processes ~~by~~ due to higher temperatures and~~shows~~ , therefore, exhibits larger $r_{\mathrm{eff,S}}$.

5.2 Case II ~~-~~ – 17 May 2012

~~On 17 May 2012 observations were analyzed between 16:45-17:12 UTC~~ For the second case, observations collected on a flight leg crossing a ~~distinct~~ sea ice edge between 16:45–17:12 UTC were analyzed. This transition allows to test the consistency of the proposed retrieval algorithm for observations over snow and open water. Compared to Case I, the cloud altitude was lower with 200 m cloud top altitude indicating a thinner cloud layer. Time of day and ~~, therefore,~~ solar zenith angle were almost identical to Case I~~and the forward simulations of the retrieval~~.

The retrieved cloud and snow properties for Case II are presented in Fig. 9. Additionally, the light gray shaded time sections indicate measurements above the open ocean while during non-shaded times snow-covered sea ice was present below the clouds. ~~To minimize the impact of 3D-radiative effects at cloud edges, corresponding to Schäfer et al. (2015) and considering the~~ As suggested by Schäfer et al. (2015) for the given cloud base and top altitude (~~0–2000~~–200 m), measurements within a distance of ~~about~~ 400 m to the sea ice edge were removed from the analysis in order to minimize the impact of 3D-radiative effects at the sea ice edge.

Over sea ice, the retrieved τ is almost constant ~~at~~ with values around 5. Across the sea ice edge, τ decreases to about 2 and later slightly increases up to $\tau = 10$ with increasing distance to the ice edge. The systematic decrease of τ over the sea ice edge as retrieved by the airborne measurements ~~extents~~ extends up to 8 km. As indicated by Schäfer et al. (2015), the radiative field across a straight sea ice edge is affected by the surface albedo transition only up to distances of about 400 m. Therefore, the coincidence of the decrease of τ with the sea ice edge ~~, observed here , can not be~~ observed here is attributed to the retrieval algorithm but rather ~~is natural . Whether,~~ has natural causes. It cannot be concluded from this single cross-section whether the change of the surface and, therefore, the change of surface latent and sensible heat fluxes ~~did affect~~ affected the cloud properties across the sea ice edge~~can not be concluded from this single cross section~~. As the high resolution MODIS observations indicate, the cloud field ~~did show an oscillation~~ showed an oscillating pattern, which might have ~~been coincidentally allocated~~ coincided with the sea ice edge at the location of the airborne observations.

The retrieved $r_{\mathrm{eff,C}}$ ~~also varies~~ vary slightly stronger over open water~~while over sea ice~~ , while the retrieved values over snow-covered sea ice are almost constant at about $r_{\mathrm{eff,C}} = 8\,\mu\mathrm{m}$ with only short ~~section~~ sections of higher cloud droplet sizes. Over open water, larger cloud droplets are found with an average of about 10 µm. Close to the sea ice edge, until 17:00 UTC, $r_{\mathrm{eff,C}}$ is found to slightly increase with increasing distance to the sea ice edge simultaneously with the increase of τ. The in situ microphysical measurements cover two cloud profiles along the same flight track, one observed above open ocean and one above sea ice. Both profiles showed no difference with $r_{\mathrm{eff,C}}$ of about 9 µm at cloud top, which are higher compared to Case I and in agreement with the retrieval results.

The retrieved $r_{\mathrm{eff,S}}$ shows a slightly higher variability and partly higher values ranging between ~~50-200~~50 µm ~~compare~~ and 200 µm compared to Case I. The larger snow grains might result from the different location, the advanced time, and snow metamorphism, or the closer location to the open water. E.g., a systematic decrease of $r_{\mathrm{eff,S}}$ with distance to the sea ice edge

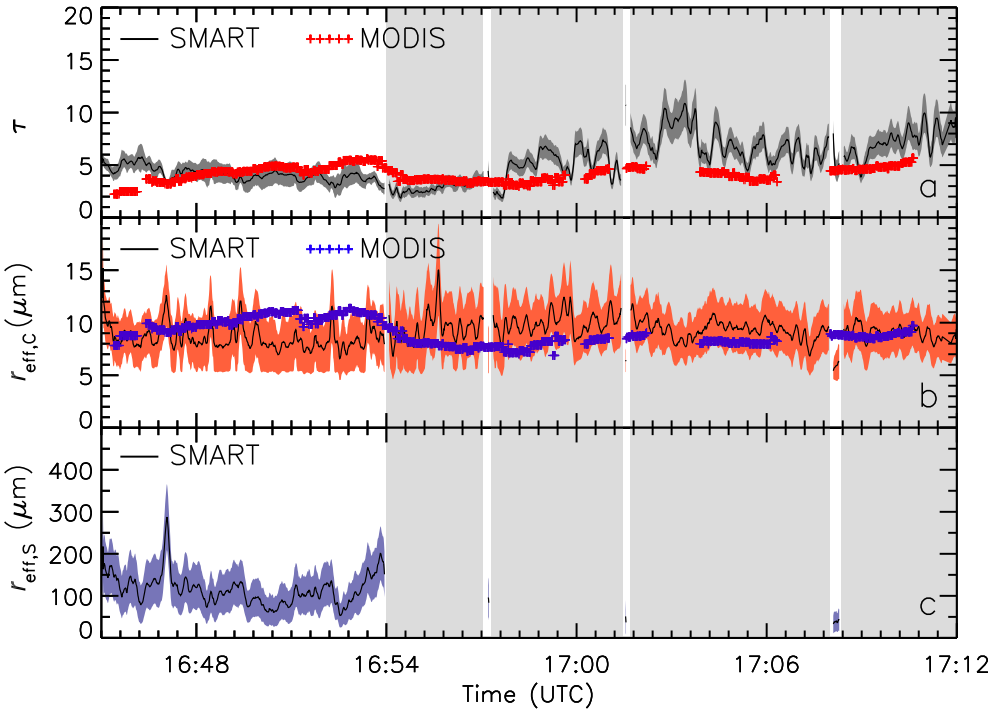

Figure 9. Same as Fig. 6 but for 17 May 2012. ~~Light gray shaded~~ Non-shaded times indicate measurements above snow while in ~~non-shades~~ light gray shaded times the ocean was ice free.

is visible (16:52-16:54 UTC, about 6 km distance). In Case II the observations are done above compact fast ice without any leads. Photographs on a flight section in the same area below the clouds showed ~~,~~ that the fast ice was partly ~~not covered by snowwhat might have cause~~ free of snow, which may have caused the higher variability and the single peak ~~with $r_{\mathrm{eff,S}}$ up to 300~~of $r_{\mathrm{eff,S}} = 300\,\mu\mathrm{m}$.

The comparison of cloud and snow properties retrieved by SMART and MODIS is shown in Figure 10 similar to Case I. MODIS results along the flight track are additionally included in Figure 9. For Case II, the MODIS image was observed at 21:25 UTC, more than 4 hours after the airborne observations. Similar to Case I, the temporal variation of the cloud properties is expected to be low as stable dynamic conditions in a high pressure system ~~did prevail~~ prevailed during the time of observations and before. Figure 10 shows that the low values of τ observed by MODIS were also covered by SMART. The slight increase of τ in the western end of the flight leg is represented by the retrieval using SMART data. A similar pattern and agreement was found for $r_{\mathrm{eff,C}}$.

The direct comparison of the time series in Figure 9 confirms the general agrement, although differences in the location of cloud fluctuations are obvious. Above sea ice, MODIS observed a steady increase of τ and $r_{\mathrm{eff,C}}$ and a similar drop at the ice edge as retrieved by SMART. However, a more quantitative comparison of SMART and MODIS cloud products is not possible

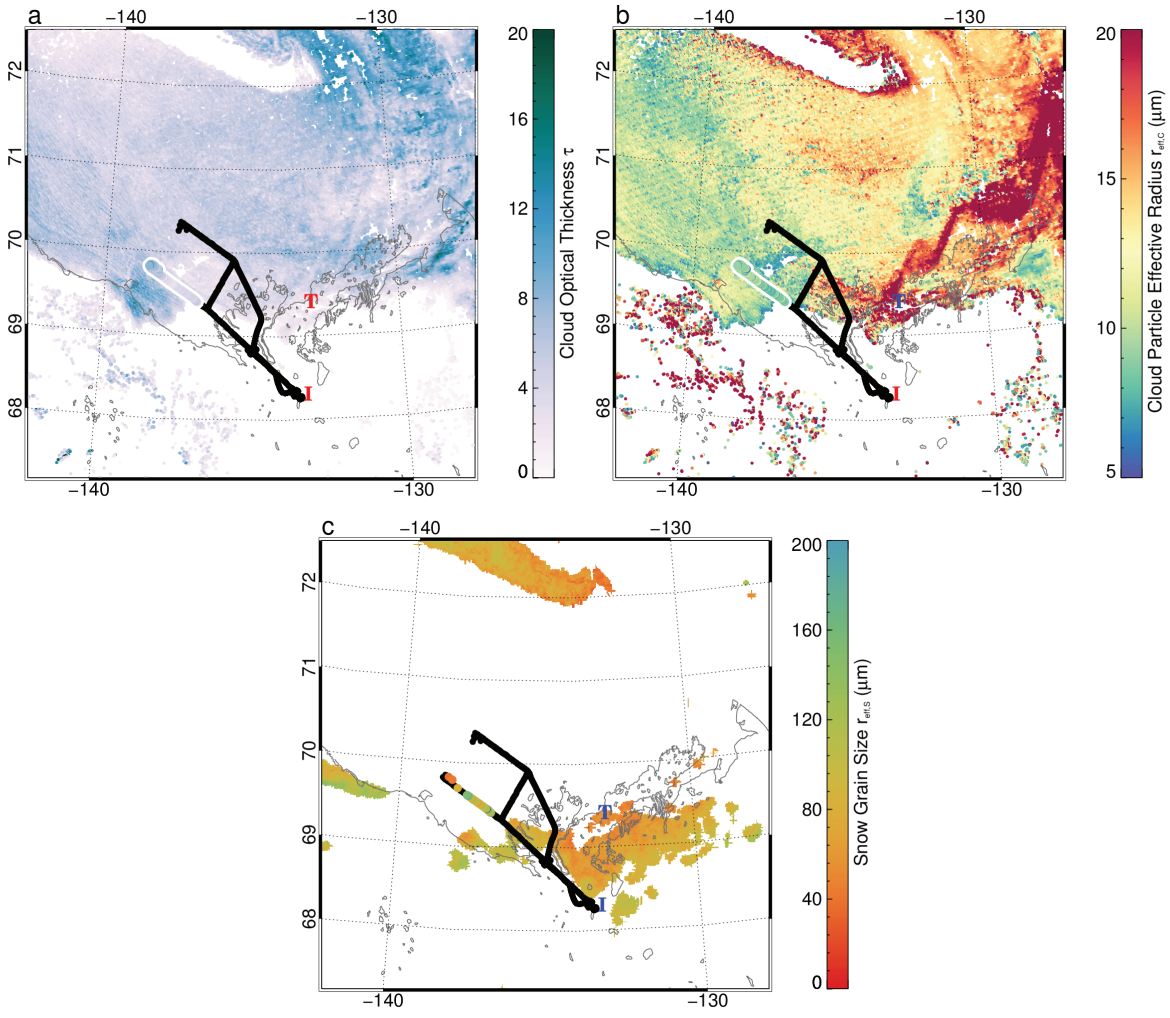

Figure 10. Same as Fig. 8 but for 17 May 2012.

due to the time difference between the observations. Differences in the retrieved cloud properties may either result from ~~a wrong~~ the assumption of snow albedo or from temporal changes of the cloud. Over open water, the MODIS cloud product provided lower τ and $r_{\mathrm{eff,C}}$. This is likely caused by the 4 hours difference between both observations. Due to the subsidence in the anticyclonic conditions the cloud top continued to decline and reduced the amount of condensed water, τ, and $r_{\mathrm{eff,C}}$. The ~~snow effective~~ effective snow grain sizes retrieved by SMART are in the range of $r_{\mathrm{eff,S}}$ retrieved by MODIS although the SGSP algorithm could provide results only in small cloud free areas. The single measurements at the western end of the flight leg indicate ~~single~~ that individual ice floes encountered on the ocean and show slightly lower $r_{\mathrm{eff,S}}$. This ~~can be~~ is an indication of fresh snow precipitation in this area where the cloud optical thickness ~~did increase~~increased.

6 Conclusions

The retrieval of cloud properties using spectral reflected solar radiation may ~~significantly be biased~~ be biased significantly if the clouds are located over a snow surface or sea ice. In this case the snow/sea ice properties have to be considered in the retrieval. An inappropriate assumption of the ~~snow effective~~ effective snow grain size results in an incorrect surface albedo at ~~non-visible wavelengths~~near-infrared wavelengths, which imprints in the retrieved cloud optical thickness and droplet effective radius. This snow grain size effect is similar to the retrieval uncertainties reported by Rolland and Liou (2001) and Fricke et al. (2014) for observations over a variable land surface albedo; only that for snow the surface albedo variability is the largest at wavelengths above roughly 1000 nm, while land surface albedo typically varies ~~in wavelengths below~~ at wavelengths less than 1000 nm.

For a ~~cloud retrieval~~ retrieval of cloud properties using similar wavelengths bands, 1600 nm and 2100 nm, as the MODIS cloud product Collection 6 applies for observations over snow or sea ice, the snow grain size effect has been quantified on the basis of radiative transfer simulations. For a typical low-level liquid water cloud ($\tau = 4$, $r_{\mathrm{eff,C}} = 10\,\mu\mathrm{m}$, $\theta_0 = 63°$) the retrieved cloud properties would differ by up to 50 % if $r_{\mathrm{eff,S}}$ is assumed to be 200 µm instead of the original ~~snow effective~~ effective snow grain size of 50 µm, or vice versa. ~~In general:~~ It is concluded:

- The snow grain size effect is largest for small snow grains because the snow albedo changes stronger in the range of small $r_{\mathrm{eff,S}}$, while for larger $r_{\mathrm{eff,S}}$ a saturation of the absorption of radiation is reached.
- The snow grain size effect on retrieved τ is almost independent of cloud optical thickness. At short wavelengths ~~,~~used to retrieve τ ($\lambda = 1600\,\mathrm{nm}$), the snow albedo is still high and always adds to the total reflected radiation. Clouds can not mask this additional reflection of the surface.
- The snow grain size effect on retrieved $r_{\mathrm{eff,C}}$ is strongest for clouds of low optical thickness. At wavelengths used to retrieve $r_{\mathrm{eff,C}}$ ($\lambda = 2100\,\mathrm{nm}$) the snow albedo is close to zero. Therefore, in case of optically thick clouds, the radiation scattered by the clouds dominates ~~the radiation~~ and can mask the additional weak reflection of the surface.
- The snow grain size effect on retrieved τ does not depend on the solar zenith angle, while the effect on $r_{\mathrm{eff,C}}$ is larger for a higher Sun.

To overcome the snow grain size effect, a method is presented that accounts for changes of the snow grain size in the retrieval algorithm for liquid water clouds~~by retrieving $r_{\mathrm{eff,S}}$ simultaneously to the cloud properties~~. A sensitivity study showed that the spectral signatures of cloud and snow properties (τ, $r_{\mathrm{eff,C}}$, $r_{\mathrm{eff,S}}$) significantly differ at specific wavelengths. Three spectral ranges were identified to be most sensitive to the three cloud and snow parameters. At wavelengths between $930 - 1350\,\mathrm{nm}$ the spectral cloud reflectivity is dominated by $r_{\mathrm{eff,S}}$, at $1500 - 1800\,\mathrm{nm}$ by τ, and at $2000 - 2300\,\mathrm{nm}$ by $r_{\mathrm{eff,C}}$.

Based on these spectral sensitivities, a retrieval algorithm was designed using reflectivity measurements at $\lambda_1 = 1040\,\mathrm{nm}$ mostly related to $r_{\mathrm{eff,S}}$, $\lambda_2 = 1650\,\mathrm{nm}$ related to τ, and $\lambda_3 = 2100\,\mathrm{nm}$ related to $r_{\mathrm{eff,C}}$. By implementing normalizations in terms of the spectral reflectivity ratios R_1, R_2, and R_3, the impact of measurement uncertainties ~~could be~~ was reduced.

The retrieval algorithm was tested in a feasibility study for airborne observations by ~~the SMART-Albedometer~~ SMART during VERDI in 2012. Two flight legs, one with closed snow-covered sea ice and a second flown across a snow-covered sea ice edge were analyzed. The results and an uncertainty analysis suggest~~the following conclusions~~:

- By considering $r_{\mathrm{eff,S}}$, retrieved τ and $r_{\mathrm{eff,C}}$ are consistent across a sea ice edge where the surface albedo ~~switches~~ changes from snow-covered sea ice to open water.
- Retrieval uncertainties depend on τ. The thicker the clouds are the stronger they will mask the surface. Less radiation is transmitted into the sub–cloud layer and can be reflected by the surface. This reduces the sensitivity and increases the uncertainties for the retrieval of $r_{\mathrm{eff,S}}$.
- Retrieval uncertainties also depend on $r_{\mathrm{eff,S}}$. Small $r_{\mathrm{eff,S}}$ increase the snow albedo and reduce the ~~contract~~ contrast between clouds and snow surface at $\lambda > 1000\,\mathrm{nm}$ increasing the uncertainties of τ and $r_{\mathrm{eff,C}}$.
- ~~Agreement with~~ Reasonable agreement between in situ cloud microphysical measurement and the MODIS cloud and snow products ~~within the limits of time differences between airborne and satellite observations~~ was found. Differences in the retrieved cloud properties may either result from a wrong assumption of snow albedo or the time difference.

For this first application of the new tri-spectral retrieval algorithm, a rather simplistic analysis was applied. A more general understanding of the retrieval sensitivities and uncertainties can be achieved by optimal estimation techniques, which is beyond of the scope of this paper. Although the retrieval was applied to cases with a specific solar zenith angle only, radiative transfer simulations showed that the spectral sensitivities used in the retrieval algorithm are similar in case of smaller or larger solar zenith angles. Therefore, the proposed retrieval method has some potential to be implemented for existing spaceborne imagers such as MODIS or VIIRS. Due to the limited number of spectral bands, for these two instrument λ_2 would have to be exchanged by the 1240 nm wavelength band where cloud reflectivity is still most sensitive to $r_{\mathrm{eff,S}}$.

By retrieving cloud properties continuously ~~also~~ along transitions from sea ice to open water ~~,~~the retrieval algorithm ~~will allow~~ allows to analyze the impact of surface changes on the cloud microphysical and optical properties. However, retrieval results close to such ice edges or in heterogeneous sea ice conditions are influenced by 3D radiative effects (Schäfer et al., 2015). For the two cases presented here, the cloud base altitude ~~and therefore also~~ was low and, therefore, the 3D radiative effects were reduced. Only a limited part of the results had to be excluded from the analysis what might differ for clouds located at higher altitudes (Schäfer et al., 2015).

The presented retrieval assumes that the surface albedo can be described by a pure snow layer of sufficient depth with no influence of the sub-snow surface. However, polar sea ice is not always covered by pure snow. Over new sea ice the snow layer might ~~be still thin and causes the sub-snow surface to reduces the albedo (Malinka et al., 2016; Warren, 2013)~~still be thin and the surface albedo reduced by the sub-snow surface (Perovich et al., 2002; Warren, 2013; Malinka et al., 2016). In the melting season, melt ponds ~~can~~ change the surface albedo (Grenfell and Perovich, 2004). Locally, melt ponds almost totally absorb solar radiation at wavelengths larger 800 nm depending on the pond depth (Lu et al., 2016). However, on larger spatial scales, the albedo of melt ponds and snow areas mix to an albedo with spectral features similar to snow of large grains sizes

(Istomina et al., 2015). For such cases, it has to be tested if the proposed retrieval algorithms still ~~can improve~~ improves the estimated cloud properties. However, the spectral signature of ~~bare~~ white sea ice and melt-pond-covered sea is ~~still~~ close to the spectral albedo of pure snow for the wavelengths used in the retrieval. In that case, the retrieved $r_{\mathrm{eff,S}}$ ~~can be~~ is interpreted as an effective snow grain size representing an arbitrary surface albedo (~~bare~~ white sea ice or melt ponds) with the same spectral characteristics above 1000 nm wavelength as a snow surface with $r_{\mathrm{eff,S}}$.

In this study ~~only liquid water dominated~~ liquid water clouds have been analyzed. However, a significant fraction of Arctic clouds are either mixed-phase or ice clouds ~~Mioche et al. (2015)~~(Mioche et al., 2015). In that case, the retrieval algorithm presented here may ~~fail~~provide unrealistic cloud properties. The ice crystals ~~in these clouds~~ absorb solar radiation at similar wavelength as the snow surface does. Therefore, the information of cloud and surface contribution to the reflected radiation might not ~~anymore~~ be sufficiently separated by the wavelengths applied here. Further sensitivity studies have to be performed to identify a different set of wavelengths that is more appropriate for the remote sensing of ice and mixed-phase clouds.

Acknowledgements. We gratefully acknowledge the support by the SFB/TR 172 "ArctiC Amplification: Climate Relevant Atmospheric and SurfaCe Processes, and Feedback Mechanisms (AC)^3" funded by the DFG ~~. We~~ (Deutsche Forschungsgesellschaft). We thank the Institute for Atmospheric Physic of the Johannes Gutenberg-Universität Mainz, in particular Stephan Borrmann and Marcus Klingebiel, for providing the in situ cloud microphysical measurements. We are grateful to the Alfred Wegener Institute Helmholtz Centre for Polar and Marine Research, Bremerhaven, Germany for supporting the VERDI campaign ~~with~~ by providing the aircraft and manpower. ~~In addition we~~ We like to thank Kenn Borek Air Ltd., Calgary, Canada for the great pilots who made the complicated measurements possible. For excellent ground support with offices and accommodations during the campaign we are grateful to the Aurora Research Institute, Inuvik, Canada.

References

Boucher, O., Randall, D., Artaxo, P., Bretherton, C., Feingold, G., Forster, P., Kerminen, V. M., Kondo, Y., Liao, H., Lohmann, U., Rasch, P., Satheesh, S. K., Sherwood, S., B., S., and Zhang, X. Y.: Clouds and Aerosols, in: Climate Change 2013: The Physical Science Basis. Contribution of Working Group I to the Fifth Assessment Report of the Intergovernmental Panel on Climate Change, edited by Stocker, T. F., Qin, D., Plattner, G. K., Tignor, M., Allen, S. K., Boschung, J., Nauels, A., Xia, V., Bex, V., and Midgley, P. M., book section 7, pp. 571–658, Cambridge University Press, Cambridge, United Kingdom and New York, NY, USA, doi:10.1017/CBO9781107415324.016, 2013.

Brückner, M., Pospichal, B., Macke, A., and Wendisch, M.: A new multispectral cloud retrieval method for ship-based solar transmissivity measurements, J. Geophys. Res.~~Atmos.~~, 119, 11.338–11.354, doi:10.1002/2014JD021775, 2014.

Dang, C., Fu, Q., and Warren, S. G.: Effect of ~~Snow Grain Shape on Snow Albedo~~snow grain shape on snow albedo, J. Atmos. Sci., 73, 3573–3583, doi:10.1175/JAS-D-15-0276.1, 2016.

Derksen, C., Lemmetyinen, J., Toose, P., Silis, A., Pulliainen, J., and Sturm, M.: Physical properties of Arctic versus subarctic snow: Implications for high latitude passive microwave snow water equivalent retrievals, J. Geophys. Res., 119, 7254–7270, doi:10.1002/2013JD021264, 2013JD021264, 2014.

Ehrlich, A., Bierwirth, E., Wendisch, M., Gayet, J.-F., Mioche, G., Lampert, A., and Heintzenberg, J.: Cloud phase identification of Arctic boundary-layer clouds from airborne spectral reflection measurements: Test of three approaches, Atmos. Chem. Phys., 8, 7493–7505, 2008.

Emde, C., Buras-Schnell, R., Kylling, A., Mayer, B., Gasteiger, J., Hamann, U., Kylling, J., Richter, B., Pause, C., Dowling, T., and Bugliaro, L.: The libRadtran software package for radiative transfer calculations (version 2.0.1), Geosci. Model Dev., 9, 1647–1672, doi:10.5194/gmd-9-1647-2016, 2016.

Flanner, M. G. and Zender, C. S.: Linking snowpack microphysics and albedo evolution, J. Geophys. Res., 111, doi:10.1029/2005JD006834, 2006.

Fricke, C., Ehrlich, A., Jäkel, E., Bohn, B., Wirth, M., and Wendisch, M.: Influence of local surface albedo variability and ice crystal shape on passive remote sensing of thin cirrus, Atmos. Chem. Phys., 14, 1943–1958, doi:10.5194/acp-14-1943-2014, 2014.

Gao, B. C., Han, W., Tsay, S. C., and Larsen, N. F.: Cloud detection over the Arctic region using airborne imaging spectrometer data during the daytime, J. Appl. Meteorol., 37, 1421–1429, doi:10.1175/1520-0450(1998)037<1421:CDOTAR>2.0.CO;2, 1998.

Grenfell, T. C. and Perovich, D. K.: Seasonal and spatial evolution of albedo in a snow-ice-land-ocean environment, J. Geophys. Res., 109, doi:10.1029/2003JC001866, c01001, 2004.

Herman, G. and Goody, R.: Formation and persistence of summertime arctic stratus clouds, J. Atmos. Sci., 33, 1537–1553, doi:10.1175/1520-0469(1976)033<1537:FAPOSA>2.0.CO;2, 1976.

Istomina, L., Heygster, G., Huntemann, M., Schwarz, P., Birnbaum, G., Scharien, R., Polashenski, C., Perovich, D., Zege, E., Malinka, A., Prikhach, A., and Katsev, I.: Melt pond fraction and spectral sea ice albedo retrieval from MERIS data – Part 1: Validation against in situ, aerial, and ship cruise data, The Cryosphere, 9, 1551–1566, doi:10.5194/tc-9-1551-2015, 2015.

Jacobi, H. W., Domine, F., Simpson, W. R., Douglas, T. A., and Sturm, M.: Simulation of the specific surface area of snow using a one-dimensional physical snowpack model: implementation and evaluation for subarctic snow in Alaska, The Cryosphere, 4, 35–51, 2010.

King, M. D., Platnick, S., Yang, P., Arnold, G. T., Gray, M. A., Riedi, J. C., Ackerman, S. A., and Liou, K. N.: Remote sensing of liquid water and ice cloud optical thickness and effective radius in the Arctic: Application of airborne multispectral MAS data, J. Atmos. Oceanic Technol., 21, 857–875, 2004.

Klingebiel, M., de Lozar, A., Molleker, S., Weigel, R., Roth, A., Schmidt, L., Meyer, J., Ehrlich, A., Neuber, R., Wendisch, M., and Borrmann, S.: Arctic low-level boundary layer clouds: in situ measurements and simulations of mono- and bimodal supercooled droplet size distributions at the top layer of liquid phase clouds, Atmos. Chem. Phys., 15, 617–631, doi:10.5194/acp-15-617-2015, 2015.

Krijger, J. M., Tol, P., Istomina, L. G., Schlundt, C., Schrijver, H., and Aben, I.: Improved identification of clouds and ice/snow covered surfaces in SCIAMACHY observations, Atmos. Meas. Technol., 4, 2213–2224, doi:10.5194/amt-4-2213-2011, 2011.

LeBlanc, S. E., Pilewskie, P., Schmidt, K. S., and Coddington, O.: A spectral method for discriminating thermodynamic phase and retrieving cloud optical thickness and effective radius using transmitted solar radiance spectra, Atmos. Meas. Tech., 8, 1361–1383, doi:10.5194/amt-8-1361-2015, 2015.

Libois, Q., Picard, G., France, J. L., Arnaud, L., Dumont, M., Carmagnola, C. M., and King, M. D.: Influence of grain shape on light penetration in snow, The Cryosphere, 7, 1803–1818, doi:10.5194/tc-7-1803-2013, 2013.

Liou, K. N., Takano, Y., He, C., Yang, P., Leung, L. R., Gu, Y., and Lee, W. L.: Stochastic parameterization for light absorption by internally mixed BC/dust in snow grains for application to climate models, J. Geophys. ~~Res. Atmos~~Res., 119, 7616–7632, doi:10.1002/2014JD021665, 2014.

Lu, P., Leppäranta, M., Cheng, B., and Li, Z.: Influence of melt-pond depth and ice thickness on Arctic sea-ice albedo and light transmittance, Cold Reg. Sci. Technol., 124, 1 – 10, doi:http://dx.doi.org/10.1016/j.coldregions.2015.12.010, 2016.

Lyapustin, A., Tedesco, M., Wang, Y., Aoki, T., Hori, M., and Kokhanovsky, A.: Retrieval of snow grain size over Greenland from MODIS, Remote Sens. Environ., 113, 1976–1987, doi:10.1016/j.rse.2009.05.008, 2009.

Malinka, A., Zege, E., Heygster, G., and Istomina, L.: Reflective properties of white sea ice and snow, The Cryosphere, 10, 2541–2557, doi:10.5194/tc-10-2541-2016, 2016.

Mioche, G., Jourdan, O., Ceccaldi, M., and Delanoe, J.: Variability of mixed-phase clouds in the Arctic with a focus on the Svalbard region: a study based on spaceborne active remote sensing, Atmos. Chem. Phys., 15, 2445–2461, doi:10.5194/acp-15-2445-2015, 2015.

Nakajima, T. and King, M.: Determination of the optical thickness and effective particle radius of clouds from reflected solar radiation measurements. Part I: Theory, J. Atmos. Sci., 47, 1878–1893, 1990.

Painter, T. H., Rittger, K., McKenzie, C., Slaughter, P., Davis, R. E., and Dozier, J.: Retrieval of subpixel snow covered area, grain size, and albedo from MODIS, Remote Sens Environ, 113, 868–879, doi:10.1016/j.rse.2009.01.001, 2009.

Perovich, D. K., Grenfell, T. C., Light, B., and Hobbs, P. V.: Seasonal evolution of the albedo of multiyear Arctic sea ice, J. Geophys. Res., 107, doi:10.1029/2000JC000438, 8044, 2002.

Pilewskie, P. and Twomey, S.: Discrimination of ice from water in clouds by optical remote sensing, Atmos. Res., 21, 113–122, 1987.

Platnick, S.: Approximations for horizontal photon transport in cloud remote sensing problems, J. Quant. Spectrosc. Radiat. Transfer, 68, 75–99, 2001.

Platnick, S., Ackerman, S. A., Baum, B. A., Heidinger, A. K., Holz, R. E., King, M. D., Menzel, W. P., Nasiri, S., Weisz, E., and Yang, P.: Assessment of IDPS VIIRS cloud products and recommendations for EOS-era cloud climate data record continuity, Tech. Rep. , p. 57, NASA Goddard Space Flight Center, Greenbelt, MD, USA, https://jointmission.gsfc.nasa.gov/DEW_NPP_reports/VIIRS/Cloud/Products/Report/(Mar-19-2013).pdf, 2013.

Platnick, S., Meyer, K. G., King, M. D., Wind, G., Amarasinghe, N., Marchant, B., Arnold, G. T., Zhang, Z., Hubanks, P. A., Holz, R. E., Yang, P., Ridgway, W. L., and Riedi, J.: The MODIS ~~Cloud Optical and Microphysical Products~~cloud optical and microphysical products: Collection 6 ~~Updates and Examples From~~ updates and examples from Terra and Aqua, IEEE Trans. Geosci. Remote Sens., 55, 502–525, doi:10.1109/TGRS.2016.2610522, 2017.

Rolland, P. and Liou, K.: Surface variability effects on the remote sensing of thin cirrus optical and microphysical properties, J. Geophys. Res., 106, 22 965–22 977, doi:10.1029/2001JD900160, 2001.

Schäfer, M., Bierwirth, E., Ehrlich, A., Jäkel, E., and Wendisch, M.: Observations and simulations of three-dimensional radiative interactions between Arctic boundary layer clouds and ice floes, Atmos. Chem. Phys. Discuss., 15, 1421–1469, doi:10.5194/acpd-15-1421-2015, 2015.

Shupe, M. D., Matrosov, S. Y., and Uttal, T.: Arctic mixed-phase cloud properties derived from surface-based sensors at SHEBA, J. Atmos. Sci., 63, 697–711, 2006.

Shupe, M. D., Walden, V. P., Eloranta, E., Uttal, T., Campbell, J. R., Starkweather, S. M., and Shiobara, M.: Clouds at Arctic ~~Atmospheric Observatories~~atmospheric observatories. Part I: Occurrence and ~~Macrophysical Properties~~macrophysical properties, J. Appl. Meteorol., 50, 626–644, doi:10.1175/2010JAMC2467.1, 2011.

Singh, P.: Snow and ~~Glacier Hydrology, Water Science and Technology Library~~glacier hydrology, water science and technology library, Springer Netherlands, 1 edn., doi:ISBN: 978-90-481-5635-1, 2001.

Stephens, G. L. and Kummerow, C. D.: The remote sensing of clouds and precipitation from space: A review, J. Atmos. Sci., 64, 3742–3765, 2007.

Vaughan, D., Comiso, J., Allison, I., Carrasco, J., Kaser, G., Kwok, R., Mote, P., Murray, T., Paul, F., Ren, J., Rignot, E., Solomina, O., Steffen, K., and Zhang, T.: Observations: Cryosphere, in: Climate Change 2013: The Physical Science Basis. Contribution of Working Group I to the Fifth Assessment Report of the Intergovernmental Panel on Climate Change, edited by Stocker, T. F., Qin, D., Plattner, G.-K., Tignor, M., Allen, S. K., Boschung, J., Nauels, A., Xia, Y., Bex, V., and Midgley, P. M., book section 4, pp. 317–382, Cambridge University Press, Cambridge, United Kingdom and New York, NY, USA, doi:10.1017/CBO9781107415324.012, 2013.

Warren, S. and Wiscombe, W.: A ~~Model for the Spectral Albedo of Snow~~model for the spectral albedo of anow. II: Snow containing atmospheric aerosols, J. Atmos. Sci., 37, 2734–2745, 1980.

Warren, S. G.: Can black carbon in snow be detected by remote sensing?, J. Geophys. Res., 118, 779–786, doi:10.1029/2012JD018476, 2013.

Warren, S. G. and Brandt, R. E.: Optical constants of ice from the ultraviolet to the microwave: A revised compilation, J. Geophys. Res., 113, Art. No. D14 220, doi:10.1029/2007JD009744, 2008.

Wendisch, M., Müller, D., Schell, D., and Heintzenberg, J.: An airborne spectral albedometer with active horizontal stabilization, J. Atmos. Oceanic Technol., 18, 1856–1866, 2001.

Wendisch, M., Brückner, M., Burrows, J. P., Crewell, S., Dethloff, K., Ebell, K., Lüpkes, C., Macke, A., Notholt, J., Quaas, J., Rinke, A., and Tegen, I.: Understanding causes and effects of rapid warming in the Arctic, Eos, 98, doi:10.1029/2017EO064803, 2017.

Werner, F., Siebert, H., Pilewskie, P., Schmeissner, T., Shaw, R. A., and Wendisch, M.: New airborne retrieval approach for trade wind cumulus properties under overlying cirrus, J. Geophys. Res. Atmos., 118, 3634–3649, doi:10.1002/jgrd.50334~~,~~, 2013.

Wiebe, H., Heygster, G., Zege, E., Aoki, T., and Hori, M.: Snow grain size retrieval SGSP from optical satellite data: Validation with ground measurements and detection of snow fall events, Remote Sens. Environ., 128, 11 – 20, doi:10.1016/j.rse.2012.09.007, 2013.

Wiscombe, W. and Warren, S.: A model for the spectral albedo of snow I. Pure snow, J. Atmos. Sci., 37, 2712–2733, 1980.

Zege, E. P., Katsev, I. L., Malinka, A. V., Prikhach, A. S., Heygster, G., and Wiebe, H.: Algorithm for retrieval of the effective snow grain size and pollution amount from satellite measurements, Remote Sens. Environ., 115, 2674–2685, doi:10.1016/j.rse.2011.06.001, 2011.